8 GaAs FET Amplifier and MMIC Design Techniques

THOMAS R. APEL*
AVANTEK, Inc., Santa Clara, California

8.1 INTRODUCTION

The objective of this chapter is to present a systematized approach to GaAs FET amplifier design. The broadband design techniques discussed here are also applicable to narrowband amplifier design as an inclusive subset. A two-stage power amplifier design is included as an example. Finally, MMIC (monolithic microwave integrated circuit) realization of lumped element designs is discussed.

With the exception of distributed amplifiers, microwave amplifiers are usually comprised of several GaAs FET devices interconnected with input, interstage, and output impedance matching networks. This is shown conceptually in Fig. 8.1. The specific amplifier application will usually determine the necessary impedance behavior which must be provided by each network. The important point here is that the methodology by which the networks are obtained remains the *same*, *regardless of application*. For example, the techniques that we are about to consider are applicable to both low-noise amplifiers and power amplifiers. They are equally applicable to single- or multistage amplifier design requirements. In fact, they also provide an effective means of insuring optimum narrowband design as well.

In order to see that the network problem for all broadband amplifier applications is really the same, several applications will be now considered. Each case will then be reduced to the (same) problem of obtaining an *LC* network with some desired driving-point impedance behavior.

1. *Low-noise amplifier*. From the optimum noise reflection coefficient ρ_{opt}, the desired matching network driving-point impedance Z_S can be determined

$$Z_S = 50 \frac{1 + \rho_{opt}}{1 - \rho_{opt}}$$

*Present address: Teledyne Monolithic Microwave, Mountainview, California.

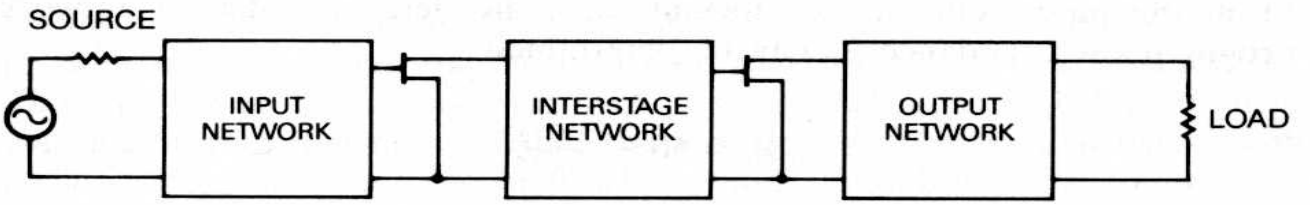

a). OVERALL MICROWAVE AMPLIFIER STRUCTURE

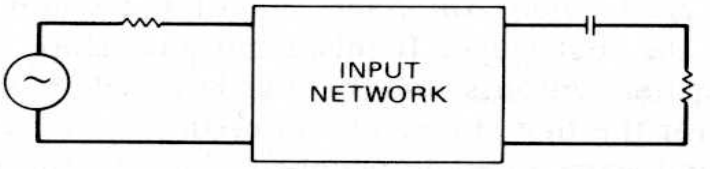

b). INPUT MATCHING PROBLEM

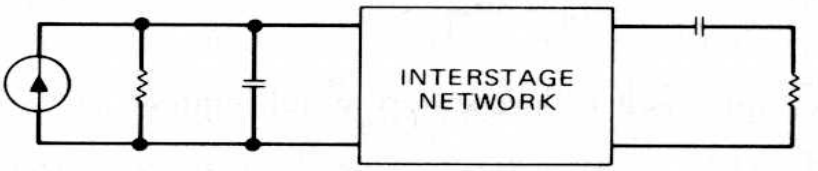

c). INTERSTAGE MATCHING PROBLEM

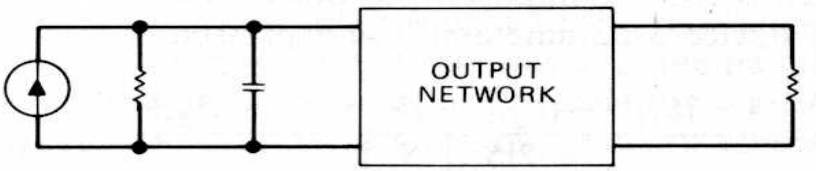

d). OUTPUT MATCHING PROBLEM

Figure 8.1 Three basic matching problems of a multi stage amplifier.

Hence, the input design requirements are in the desired form. Flat amplifier gain can be achieved by controlled mismatch at the output port of the device. Typically, constant gain circles are plotted for this interface. A desired load impedance Z_L is then determined. Therefore, the output matching network is also specified in the desired form.

2. *Power Amplifier.* Either from load line considerations or load–pull data the optimum load impedance $Z_{L\,opt}$ is determined. The design task is to obtain an output matching network that provides this optimum load impedance behavior. Usually, minimum input port reflection is desired. The device input reflection coefficient S'_{11} is determined:

$$S'_{11} = S_{11} + \frac{S_{12}S_{21}\rho_{L\,opt}}{1 - S_{22}\rho_{L\,opt}}$$

From the input reflection coefficient S'_{11}, the desired matching network driving-point impedance Z_S can be determined:

$$Z_S = 50 \frac{1 + S'^*_{11}}{1 - S'^*_{11}}$$

So, the input matching network design requirements are also in the desired form.

3. *Interstage of High Gain Amplifier.* S'_{11} of the second stage must be matched to S'_{22} of the first stage. If mismatch gain slope compensation is desired, constant gain contours can be used to select the desired load impedance $Z_{L\,opt}$, for the first stage. The interstage matching network must transform the second-stage input impedance Z_{IN} into the desired load for the first stage, $Z_{L\,opt}$:

$$Z_{IN} = 50 \frac{1 + S'_{11}}{1 - S'_{11}}$$

Detailed design examples will be presented in subsequent sections.

8.2 STABILITY AND GAIN

Rollette's stability constant k is important to practical GaAs FET amplifier design. In terms of device S-parameters, it is expressed as

$$k = \frac{1 - |S_{11}|^2 - |S_{22}|^2 - |S_{11}S_{22} - S_{12}S_{21}|^2}{2|S_{21}|\,|S_{12}|}$$

Although one-port unilateral models (as seen in Fig. 8.27) are frequently used to represent impedance matching requirements, the complete device representation is nonunilateral. Therefore, at frequencies at which useful gain is available, the potential for oscillations must be examined. Even for power amplifier applications, where the device is being operated nonlinearly, small-signal stability should also be considered.

The significance of Rollette's stability constant is that for $k > 1$, the device is unconditionally stable and no combination of load and source impedances can produce oscillations. For this case, simultaneous complex conjugate matching of the FET input and output ports is possible. When this is done, maximum available gain (MAG) results. The expression for MAG is given by

$$\text{MAG} = \frac{|S_{21}|}{|S_{12}|}\,(k - \sqrt{k^2 - 1})$$

If, on the other hand, $k < 1$, some load and source impedances can cause

oscillations. In such cases, the impedance regions to be avoided can be plotted or represented graphically by circular regions on the Smith chart. This method is adequately described in several references [1, 2]; hence, it will not be repeated here. Often, these difficulties are avoided when lossy negative feedback or lossy branch amplitude equalization techniques are employed. The lossy branch technique will be discussed in the two-stage design example of Section 8.4.4.

8.3 Q-BANDWIDTH LIMITS ON IMPEDANCE MATCH

Before any attempt to design a broadband matching network, the achievable match performance must first be determined. A common pitfall that the inexperienced circuit designer often encounters is an attempt to obtain matching networks blindly by numerical optimization. If the desired performance level is not achievable, considerable computer and engineering time can be wasted. This section addresses the limits imposed on impedance match performance by load behavior.

The relative reactive to resistive (susceptive to conductive) behavior of the load immittance sets the limits on achievable broadband performance. This behavior is sometimes described in terms of a parameter called load-Q. Bode [3] showed that the integral of return loss is bound by a constant. This constant is dependent on the behavior of the reflection function. The load that was initially considered by Bode was a simple parallel RC. In this case, the match performance limit can be described in terms of load-Q and the complex frequency location of matching network reflection function zeros. Several years later, Fano [4] extended Bode's work to address more general cases. For our purposes here, a detailed look at Bode's work will suffice. In addition to the parallel RC case that Bode considered, we will show that the circuit-dual (series RL case) also yields the same results. So, all single reactance absorption lowpass cases are covered. These results can then be extended to the two-element bandpass cases by the well-known lowpass to bandpass transformation.

The two cases that will now be considered are illustrated in Fig. 8.2. An LC matching network that absorbs to complex valued load behavior and provides an impedance-matched filter response to the R_0 source is desired. Matching networks are filter structures. However, a filter that provides a low reflection match between a resistive source and load is not necessarily a matching network. The additional requirement that is imposed on matching networks is reactance absorption at one or both sides of the structure. Typical filter responses have zero flat-loss (offset) due to reflection zeros on the imaginary axis. Since matching networks have additional constraints placed on them, additional degrees of freedom in the realization are required. General placement of reflection zeros allows this freedom. The

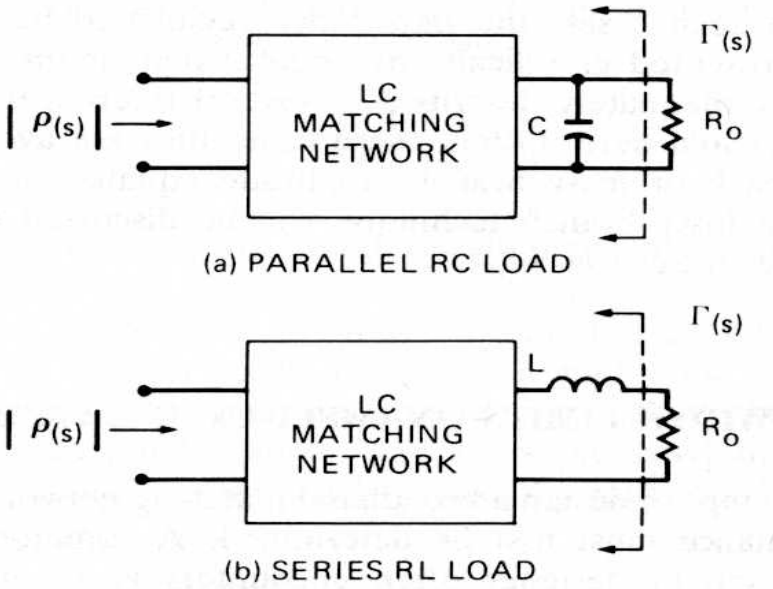

Figure 8.2 Load representations for match limit analysis.

significance of which half of the complex plane the zeros are placed will become clear when Eq. (13) is discussed.

The match limit relationships that we seek are obtained by considering the following contour integral:

$$\oint \log \left| \frac{1}{\rho'} \right| dS$$

where the path of integration is the simple closed contour shown in Fig. 8.3. The reflection function in the above expression is related to the reflection function in Fig. 8.2 by

$$\rho' = \rho \frac{(S + S_1)(S + S_2)(- - -)(S + S_n)}{(S - S_1)(S - S_2)(- - -)(S - S_n)} \tag{1}$$

Both functions have identical steady-state magnitude, since they differ only by an allpass factor. Equation (1) provides a convenient means of accounting for any right-half plane (RHP) zeros of ρ. Since the contour integral contains the reciprocal of Eq. (1) in the integrand, zeros of ρ' represent poles in the integrand. The allpass factor allows the presence of any RHP zeros of ρ to be removed from ρ' without changing the steady-state magnitude characteristic. For each RHP zero of ρ, S_i, A corresponding RHP pole and LHP zero appear in the allpass function. This integral can be expressed in two parts, by considering the closed contour in two segments, as seen in[†]

$$\oint \log \left| \frac{1}{\rho} \right| dS = j \int_{-\infty}^{\infty} \log \left| \frac{1}{\rho} \right| d\omega + \int \lim_{|S| \to \infty} \log \left| \frac{1}{\rho} \right| dS \tag{2}$$

[†] (Editor's Note): ρ and ρ' have same steady state magnitude.

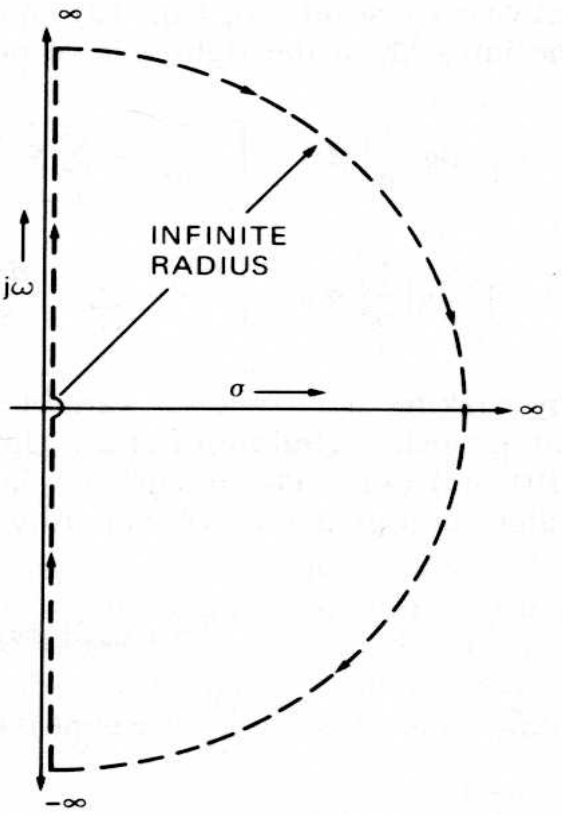

Figure 8.3 Contour integration.

Hence, no RHP poles appear in the integrand. By the Cauchy–Goursat theorem, the integral is zero. This leads to Eq. (3), or in admittance form Eq. (4).

$$-2j\int_0^\infty \log\left|\frac{1}{\rho}\right| d\omega = \int \lim_{|S|\to\infty} \log\left|\frac{1+Z_L/R_0}{1-Z_L/R_0}\right| + \lim_{|S|\to\infty}\sum_i \log\left|\frac{1-S_i/S}{1+S_i/S}\right| dS \qquad (3)$$

$$-2j\int_0^\infty \log\left|\frac{1}{\rho}\right| d\omega = \int \lim_{|S|\to\infty} \log\left|\frac{1-Y_L/G_0}{1+Y_L/G_0}\right| + \lim_{|S|\to\infty}\sum_i \log\left|\frac{1-S_i/S}{1+S_i/S}\right| dS \qquad (4)$$

The infinite radius limits of the load impedance and admittance for the RC and RL cases are presented in Eqs. (5) and (6), respectively. Similarly, the infinite radius limit of the allpass factors are presented in Eq. (7).

$$\lim_{|S|\to\infty} \log\left|\frac{1+Z_L/R_0}{1-Z_L/R_0}\right| = \frac{2}{SR_oC} \qquad (5)$$

$$\lim_{|S|\to\infty} \log\left|\frac{1-Y_L/G_0}{1+Y_L/G_0}\right| = \frac{2R_o}{SL} \qquad (6)$$

$$\lim_{|S|\to\infty} \log\left|\frac{1-S_i/S}{1+S_i/S}\right| = -2\frac{S_i}{S} \qquad (7)$$

By making these limit case substitutions, Eqs. (3) and (4) yield Eqs. (8) and (9), respectively. The integral on the right side of both

$$-j\int_0^\infty \log\left|\frac{1}{\rho}\right| d\omega = \int \frac{1}{CR_0} - \sum_i S_i \frac{dS}{S} \tag{8}$$

$$-j\int_0^\infty \log\left|\frac{1}{\rho}\right| d\omega = \int \frac{R_0}{L} - \sum_i S_i \frac{dS}{S} \tag{9}$$

can be evaluated by making a change in variables and performing the integration in theta at a constant (infinite) radius. This change in variables is indicated in Eqs. (10) and (11). The integration in a clockwise direction around the semicircular contour is then obtained by Eq. (12).

$$S = r\exp(j\Theta) \tag{10}$$

$$\frac{dS}{d\Theta} = jr\exp(j\Theta) \tag{11}$$

$$\int_{\pi/2}^{-\pi/2} \frac{jr\exp(j\Theta)}{r\exp(j\Theta)}\, d\Theta = -j\pi \tag{12}$$

Hence, the results of Eq. (13) are obtained. This is Bode's limit. We can clearly see from this that the presence of any RHP reflection zeros will degrade the match performance. Later, it will be demonstrated that RHP zeros allow greater reactance absorption at the source side of the matching network. This zero-placement trade-off is important in the design of interstage matching networks, where reactance absorption at both ports is important.

$$\int_0^\infty \log\left|\frac{1}{\rho}\right| d\omega = \frac{\pi}{CR_0} - \pi\sum_i S_i \tag{13a}$$

$$\int_0^\infty \log\left|\frac{1}{\rho}\right| d\omega = \frac{\pi L}{R_0} - \pi\sum_i S_i \tag{13b}$$

From Eq. (13), it is clear that with LHP zero placement the integral of return loss is equal to a constant that is inversely proportional to load-Q. Consider Fig. 8.4. The area under the curve represents the value of the integral. If load-Q is decreased, the available area is correspondingly increased; so, the same level of match performance is achievable over a wider band. It is also true that if the load-Q is unchanged, a reduction in

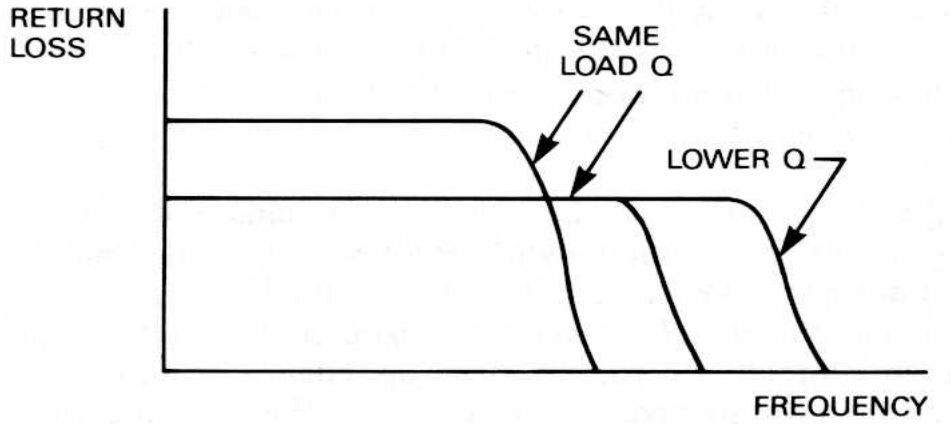

Figure 8.4 Q-Bandwidth trade-off.

desired bandwidth permits an improvement in match performance. These qualitative observations are intuitive. Equation (13) is important because it allows a quantitative assessment. Sometimes Bode's limit is expressed with the inequality seen in Eq. (14). This result is easily obtained from both forms of Eq. (13) with LHP zeros and ideal "brick wall" lowpass amplitude response.

$$|\rho| \geq \exp(-\pi/Q_L) \tag{14}$$

Clearly, to make use of Eq. (13) or (14), a lumped model that represents the load impedance behavior is required. Load modeling techniques and the bandpass equivalent of Eqs. (14) will be detailed in Sections 8.4.3 and 8.4.2.1, respectively.

8.4 BROADBAND MATCHING NETWORK DESIGN

The design of lumped LC impedance matching networks is now considered. Applicability of the approach to be discussed is wide-ranging, since most practical applications can be reduced to the problem of obtaining some desired impedance behavior at one or both sides of a two-port network.

Direct distributed synthesis techniques, such as those using the Richards transformation and Kuroda identities, will not be considered here. This was decided for several reasons:

1. Discontinuities are not accounted for in distributed synthesis.
2. Lumped designs can be easily converted to an equivalent distributed form.
3. Discontinuities can be folded into the design at the lumped-to-distributed conversion step.

4. Commensurate element designs are virtually always larger and therefore more lossy and less desirable for monolithic integration.
5. Reactance absorption requires unit elements to be inserted only from one side of the network.

It is important to note that there are two fundamentally different ways of addressing the *LC* matching network problem. One is the more classic filter synthesis approach, which requires that a load model be available for absorption into the matching network through the synthesis process. The other operates directly on the interface impedance requirements without a model. The material presented here falls into the first category.

The classic filter synthesis approach to broadband impedance matching network design usually involves four activities:

1. *Approximation*: a functional representation of the desired response.
2. *Realization*: the network synthesis step that satisfies the approximation and absorbs the load model.
3. *Mapping*: a frequency domain transformation to the desired passband.
4. *Load Model*: a one-port formed by an *LC* two-port that is resistively terminated.

These four aspects are discussed in the next three subsections.

8.4.1 The Lowpass Prototype

Although most design requirements are for passbands that do not extend down to dc, the lowpass representation is very useful. Since frequency domain mappings can be used to extend approximations to other bands, it is not necessary to address the approximation problem separately for each type of network to be considered. In some cases, even the completed network realizations can be transformed directly. The lowpass (LP) to bandpass (BP) mapping is one such case.

It is clear that an optimum matching network will only provide good matching inside the desired passband. This is a consequence of the Bode analysis, since the area under the return-loss frequency response is fixed. One of several classic approximations can be applied here to achieve an abrupt transition between passband and stopband. Usually, the phase-transfer characteristic is not a primary consideration. Cases in which phase linearity is important can have additional bandwidth margin designed in or use another approximation, such as the Bessel or Gaussian. Of potential interest here are the Butterworth, Chebyshev, and elliptic responses. Each of these has previously been used for matching network design. However, the Chebyshev (equal-ripple) response is by far the most popular because it offers superior performance to the Butterworth form and is more easily

realized than the elliptic form. Consequently, the sensitivity to element variations also falls between the Butterworth and elliptic cases. This section will consider the Chebyshev LP approximation and LP prototype synthesis.

The LP prototype network is frequency- and impedance-normalized. The general Chebyshev amplitude-transfer function is illustrated in Fig. 8.5. Note that in addition to ripple loss, allowance has been made for nonzero offset loss (flat loss). This is represented algebraically in Eq. (15) the expression for insertion loss, where T_N is the Nth Chebyshev polynomial of the first kind:

$$|IL|^2 = 1 + K^2 + \epsilon^2 T_N^2(\Omega) \tag{15}$$

Since insertion loss in LC ladder networks is due to reflection, the reflection function ρ is representable as a function of the desired insertion-loss response. This relationship is expressed in Eq. (16) and from it Eq. (17) follows:

$$|\rho|^2 = \frac{|IL|^2 - 1}{|IL|^2} \tag{16}$$

$$|\rho|^2 = \frac{(K/\epsilon)^2 + T_N^2}{(1 + K^2)/\epsilon^2 + T_N^2} \tag{17}$$

The roots of the numerator and denominator of Eq. (17) allow the reflection zeros and poles to be determined. In order to represent a realizable network, the poles are restricted to the LHP. The only restriction placed on the zeros of reflection is that they must appear in complex conjugate pairs or on the real axis. Note that reflection zeros may appear in RHP or LHP, and the *same* magnitude insertion-loss response may be achieved. The network

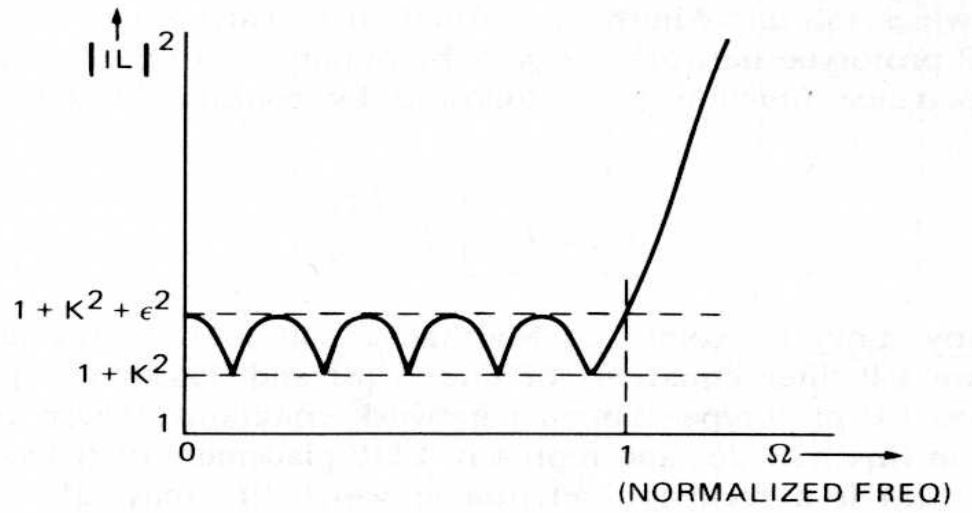

Figure 8.5 Chebyshev LP prototype response.

element values will be affected, since symmetric (with respect to the imaginary axis) reflection zero shifts result in an interchange in the port Q's. The S-plane poles and zeros of reflection are represented in Eqs. (18–21), where i is an integer between 1 and N. The subscript pi or zi is used to indicate the ith pole or zero, respectively.

$$S_{pi} = -\sin\left[\frac{\pi(2i-1)}{2N}\right]\sinh[a] \pm j\cos\left[\frac{\pi(2i-1)}{2N}\right]\cosh[a] \tag{18}$$

$$S_{zi} = -\sin\left[\frac{\pi(2i-1)}{2N}\right]\sinh[b] \pm j\cos\left[\frac{\pi(2i-1)}{2N}\right]\cosh[b] \tag{19}$$

$$a = \frac{1}{N}\sinh^{-1}\left(\sqrt{\frac{1+K^2}{\epsilon^2}}\right) \tag{20}$$

$$b = \frac{1}{N}\sinh^{-1}\left(\frac{K}{\epsilon}\right) \tag{21}$$

Equations (20) and (21) provide two constants (a and b) called Fano's parameters, which appear in Eqs. (18) and (19). One should not be surprised to find that there is a unique combination of response offset (K^2) and ripple (ϵ^2) that provides a *minimum* mismatch loss in passband. This optimum case is sometimes called the Fano match case. The corresponding Fano parameter values are given in Figs. 8.6 and 8.7 as a function of LP prototype load-Q. Our purpose here is to provide a practical means of designing optimum wideband circuits with a minimum of esoteric complexity. Intentionally, the class of LP loads has been limited to single reactance cases, since Matthaei's [5] "situation 1" can thereby be ensured. The reader should keep in mind that this allows freedom for two-element bandpass models. The bandpass load modeling technique that will be presented in Section 8.4.3 provides a means of ensuring that fourth-order models can be obtained which fall into Matthaei's "situation 1" category.

The LP prototype network can now be obtained by forming the driving-point impedance function (22), followed by continued fraction [6] expansion:

$$Z_{dp}(S) = \frac{1+\rho(S)}{1-\rho(S)} \tag{22}$$

Significantly, Levy [7] combined Matthaei's "situation 1" results with the closed-form LP filter equations of Green [8] and Takahasi [9] to obtain closed-form LP prototype matching network equations. These expressions are given in Eqs. (23–26) and represent LHP placement of reflection zeros. Equation (25) is a recursion relation in which "i" may take on integer values between 1 and $N-1$, for an Nth-order network.

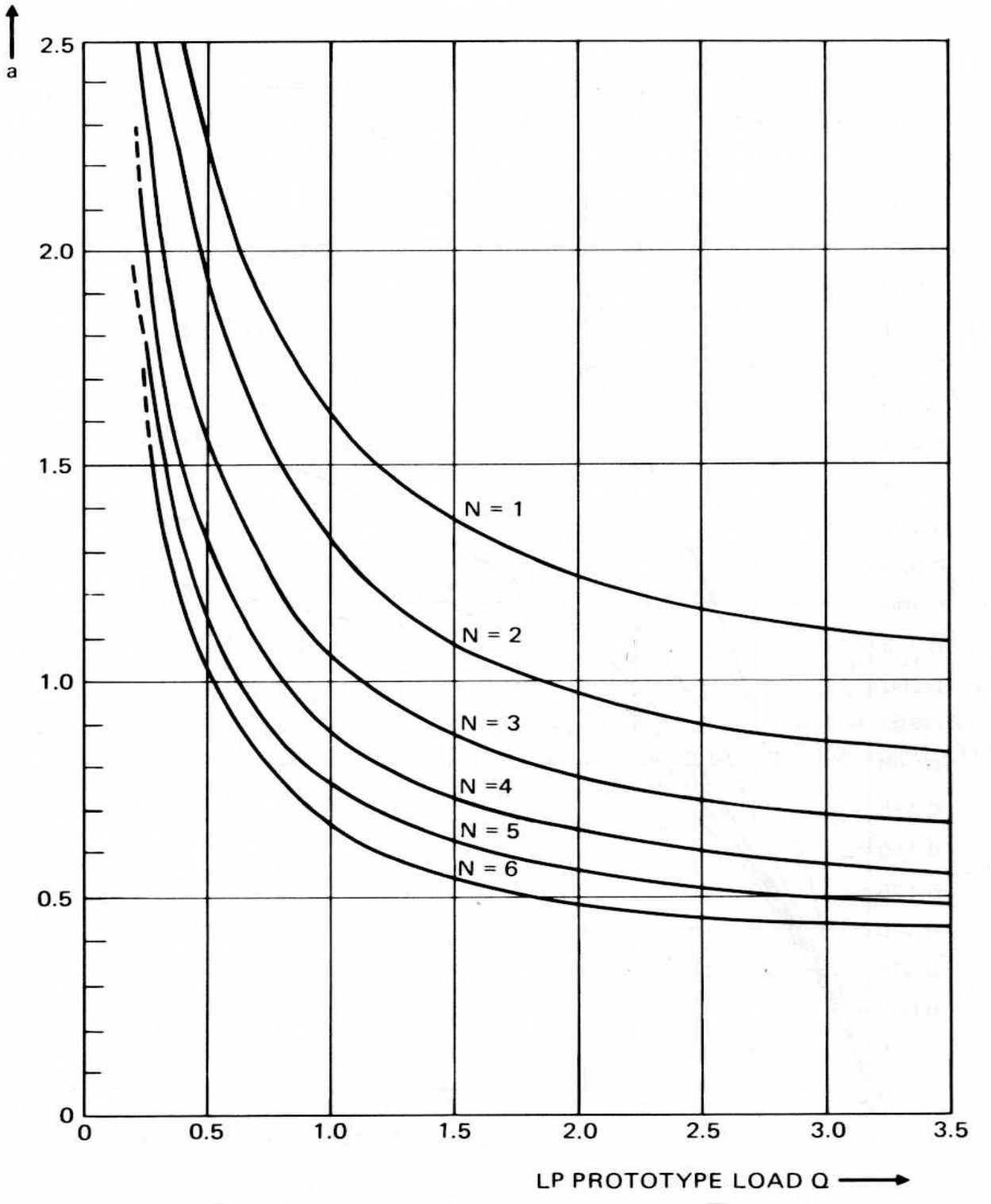

Figure 8.6 Fano's *a* parameter.

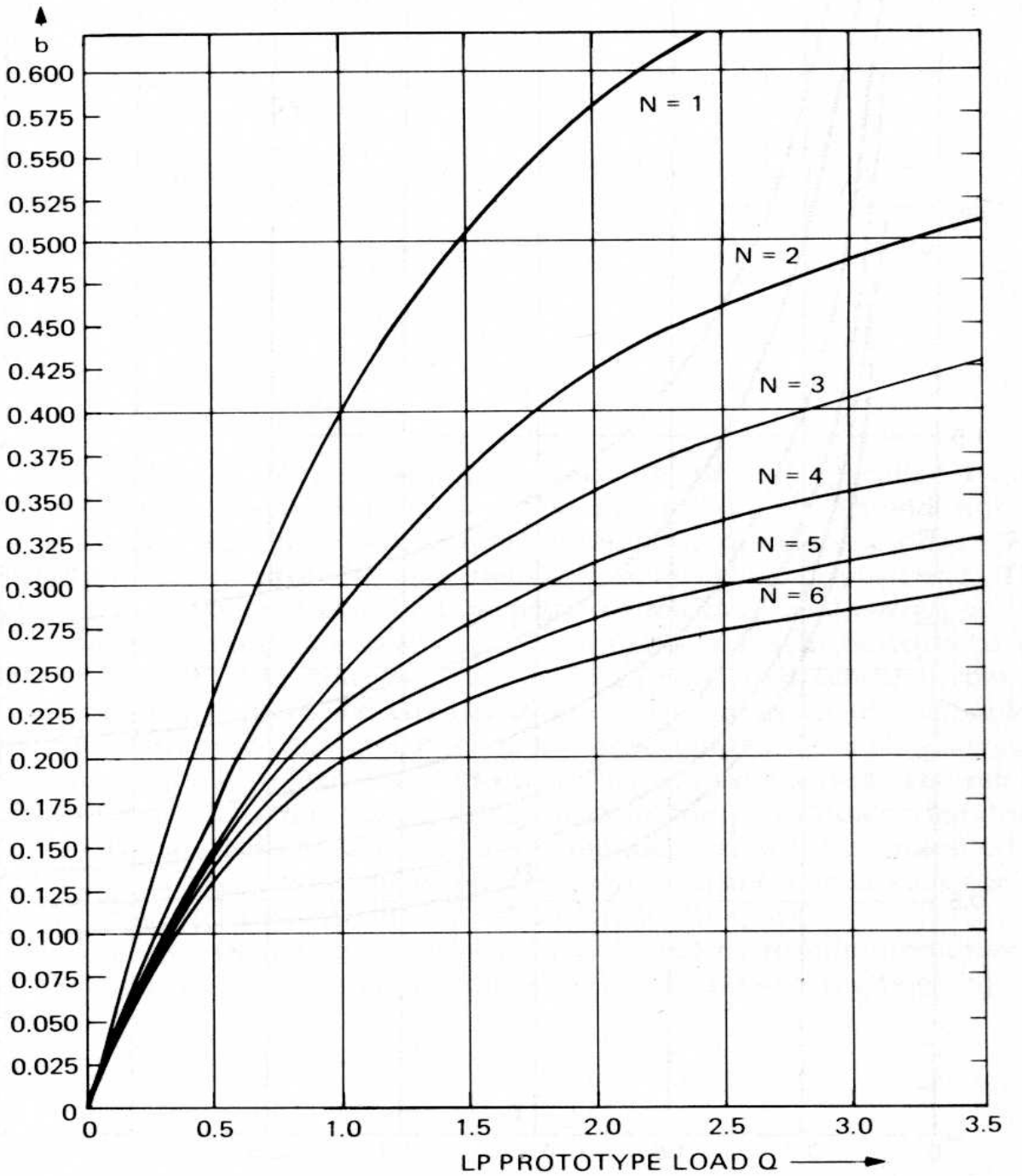

Figure 8.7 Fano's *b* parameter.

$$g_0 = 1 \tag{23}$$

$$g_1 = \frac{2\sin[\pi/(2N)]}{\sinh[a] - \sinh[b]} \tag{24}$$

$$g_i g_{i+1} = \frac{4\sin[\pi(2i-1)/(2N)]\sin[\pi(2i+1)/(2N)]}{\sinh^2[a] + \sinh^2[b] + \sin^2[\pi i/N] - 2\sinh[a]\sinh[b]\cos[\pi i/N]} \tag{25}$$

$$g_N g_{N+1} = \frac{2\sin[\pi/(2N)]}{\sinh[a] + \sinh[b]} \tag{26}$$

At this point, we note that $g_0 g_1$ and $g_N g_{N+1}$ are load and source Q, respectively. For convenience, they will be denoted Q_L and Q_S. It should be noted that Eqs. (24) and (26) can be solved simultaneously for Fano's a and b when Q_S and Q_L are both specified. This provides a means of designing interstage matching networks, as seen in Eqs. (27) and (28):

$$a = \sinh^{-1}\left\{\sin\left[\frac{\pi}{2N}\right]\left(\frac{1}{Q_L} + \frac{1}{Q_S}\right)\right\} \tag{27}$$

$$b = \sinh^{-1}\left\{\sin\left[\frac{\pi}{2N}\right]\left(\frac{1}{Q_S} - \frac{1}{Q_L}\right)\right\} \tag{28}$$

From a substitution of Eqs. (20) and (21) into Eq. (17), we obtain Eq. (29). By evaluating this expression at $T_N = 0$ and $T_N = 1$, expressions for the minimum and maximum reflection coefficients are obtained for this Nth-order case. These match limit results, which are seen in Eqs. (30) and (31), complement the previously discussed Bode limit.

$$|\rho|^2 = \frac{\sinh^2[Nb] + T_N^2}{\sinh^2[Na] + T_N^2} \tag{29}$$

$$|\rho|_{\min} = \frac{\sinh[Nb]}{\sinh[Na]} \tag{30}$$

$$|\rho|_{\max} = \frac{\cosh[Nb]}{\cosh[Na]} \tag{31}$$

A LOWPASS MATCH EXAMPLE

Before moving on to the more important consequences of the preceding LP formulation, an example of a LP matching network is in order.

Suppose we wish to obtain a baseband (video) match from dc to 10 MHz into a parallel load that is comprised of a 1000 pF capacitor and a 31.8 Ω resistor. Use a third-order matching network.

Match Limits: $Q_L = (2\pi 10^7)(10^{-9}\ F)(31.8\ \Omega) = 2.0$

$$\text{Rho}_{\text{Bode}} = \exp\left(\frac{-\pi}{2}\right) = 0.208$$

$$\text{VSWR}_{\text{Bode}} = 1.5{:}1$$

$$\text{VSWR}_{\text{min}} = 1.66{:}1$$

$$\text{VSWR}_{\text{max}} = 1.90{:}1$$

Fano Parameters: $a = 0.783$

$b = 0.358$

LP Prototype: $g_0 = 1.0\ \Omega$

$g_1 = 2.0\ \text{F}$

$g_2 = 0.760\ \text{H}$

$g_3 = 1.351\ \text{F}$

$g_4 = 0.602\ \Omega$

Denormalized LP Prototype: Frequency scale by $2\pi\ 10^7$

Impedance scale by 31.8

Hence, the LP matching network shown in Fig. 8.8 is obtained:

(From g_0) $R_L = 31.8\ \Omega$

(From g_1) $C_1 = 1000\ \text{pF}$

(From g_2) $L_1 = 0.385\ \mu\text{H}$

(From g_3) $C_2 = 677\ \text{pF}$

(From g_4) $R_s = 19.12\ \Omega$

Note that the desired load model was forced. This occurred through the selection of the Fano parameters and LHP zero placement, which ensured

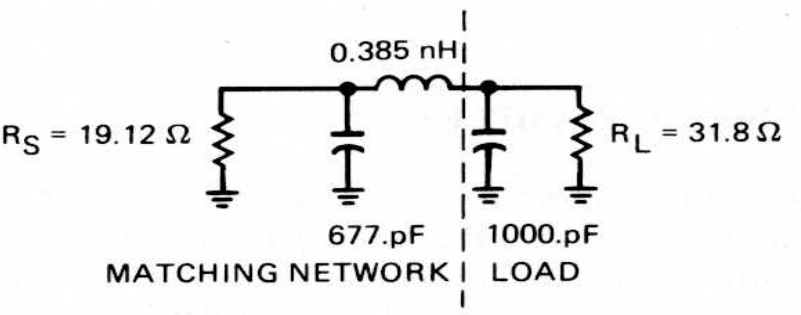

Figure 8.8 LP match example.

optimum performance with this load-Q. Unfortunately, the LP matching procedure does not provide a means of adjusting the source resistance, since transformers (and transformer equivalent circuits) do not function at dc. The networks obtained by the frequency transformation in the next section do not share this limitation.

8.4.2 Mappings

When impedance matching down to dc is not required, as is usually the case, a number of frequency transformations can be applied to the LP formulation. Three mappings are considered in this section: the bandpass BP, the degree doubling quasi-lowpass QLP, and the degree doubling quasi-highpass QHP.

8.4.2.1 Lowpass-to-Bandpass Transformation. Perhaps the most well-known frequency transformation is the LP to BP. It is illustrated in Fig. 8.9, and defined in Eq. (32), where S and p are the LP and BP complex frequencies, respectively. The transform Q, Q_T, is defined in Eq. (33), with passband corner frequencies f_1 and f_2.

$$S = Q_T\left[\frac{\omega_0}{p} + \frac{p}{\omega_0}\right] \tag{32}$$

$$Q_T = \frac{\sqrt{f_2 f_1}}{f_2 - f_1} \tag{33}$$

Reflection functions, pole and zero locations, and transfer functions can all be transformed to BP form with Eq. (32). However, the most surprising feature of this mapping is that it allows network conversions on an element-by-element impedance basis! Consider an inductor of LP complex impedance SL. Two impedance terms result when Eq. (32) is applied: $(Q_T\omega_0 L)/p + (Q_T L/\omega_0)p$. The first term appears to be a capacitor equal to $1/(Q_T\omega_0 L)$, while the second term behaves as an inductor equal to $(Q_T L/\omega_0)$.

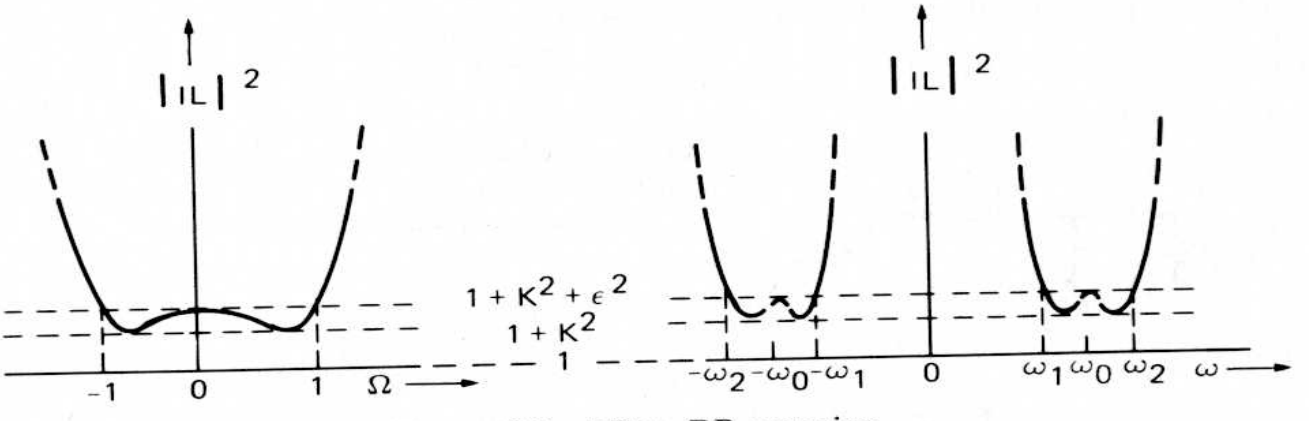

Figure 8.9 LP to BP mapping.

Hence, a series LC branch results from a LP inductor. Similarly, a capacitor of LP complex admittance SC will yield two terms under this mapping. The first will appear as an inductor equal to $1/(Q_T\omega_0 C)$. In parallel with this inductor is a capacitor equal to $(Q_T C/\omega_0)$, contributed by the second susceptance term. So, LP capacitors map into parallel LC branches. The inductors in the series resonators and the capacitors in the parallel resonators are obtained numerically by frequency scaling the corresponding LP prototype elements by the desired bandwidth, in radian frequency. The associated branch element is obtained by setting the resonance at midband (geometric center). Figure 8.10 illustrates the possible LP prototype to BP network relationships.

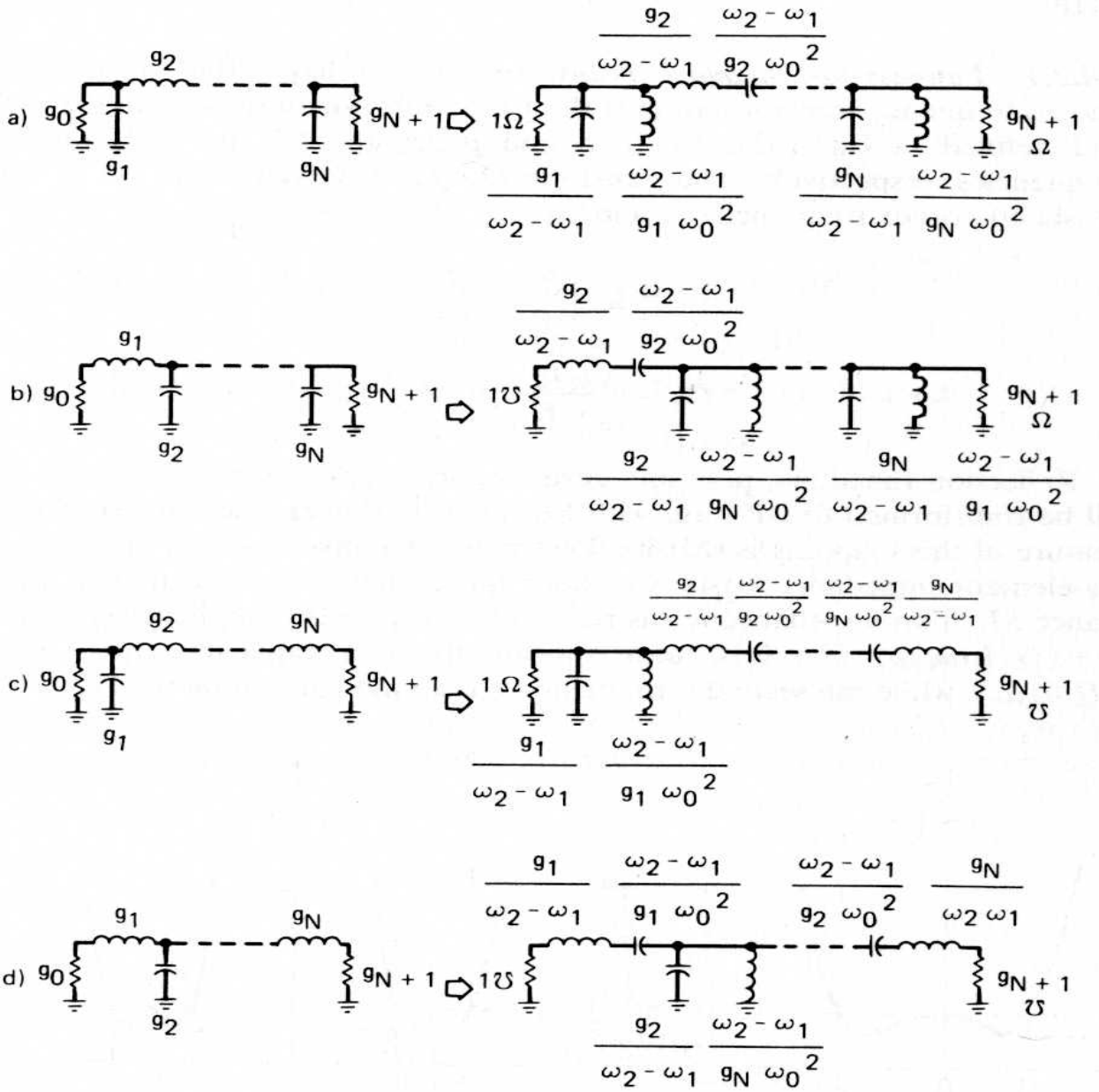

Figure 8.10 LP prototype to BP elements.

Since the requirements (of Q_L and impedance level) present at the load side of the bandpass network necessary to force the desired load model usually do not provide the desired source resistance, additional transformer action is needed. Clearly, it can now be seen that broadband matching is comprised of two distinct actions: reactance absorption and impedance transformation. Usually, both are required for a complete impedance match. The need for transformers is satisfied by Norton [10] subcircuits, discussed next.

The Norton transformer subnetworks are comprised of an ideal transformer cascaded with a pair of series- and shunt-connected inductors or capacitors. Figure 8.11 illustrates the subnetworks that will be considered. They are realized with equivalent "T" or "pi" structures. The "T" equivalents are obtained by coefficient matching Z-parameter representations. Similarly, coefficient matching in Y-parameter form yields the pi structures.

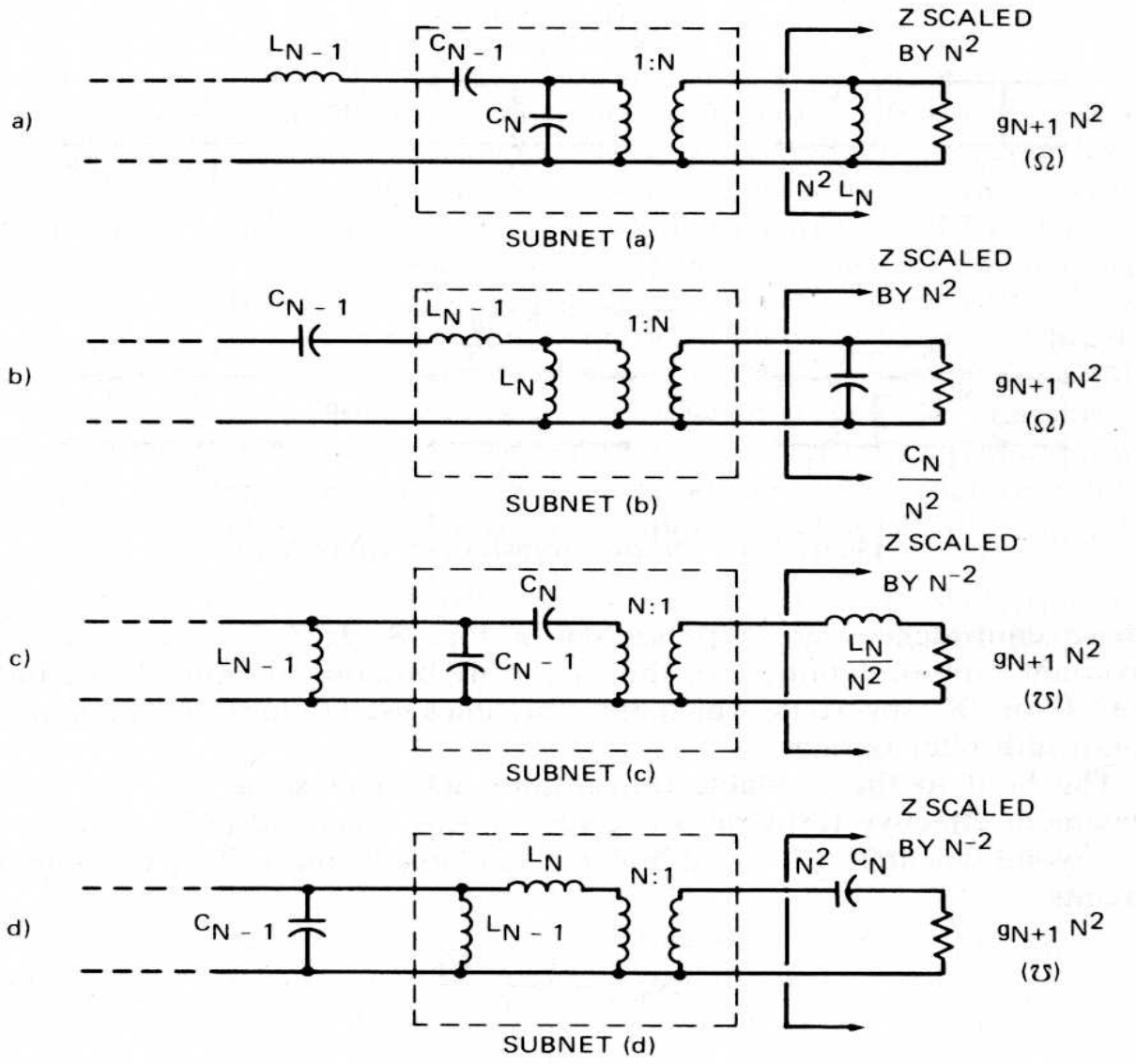

Figure 8.11 Norton transformer subnetworks.

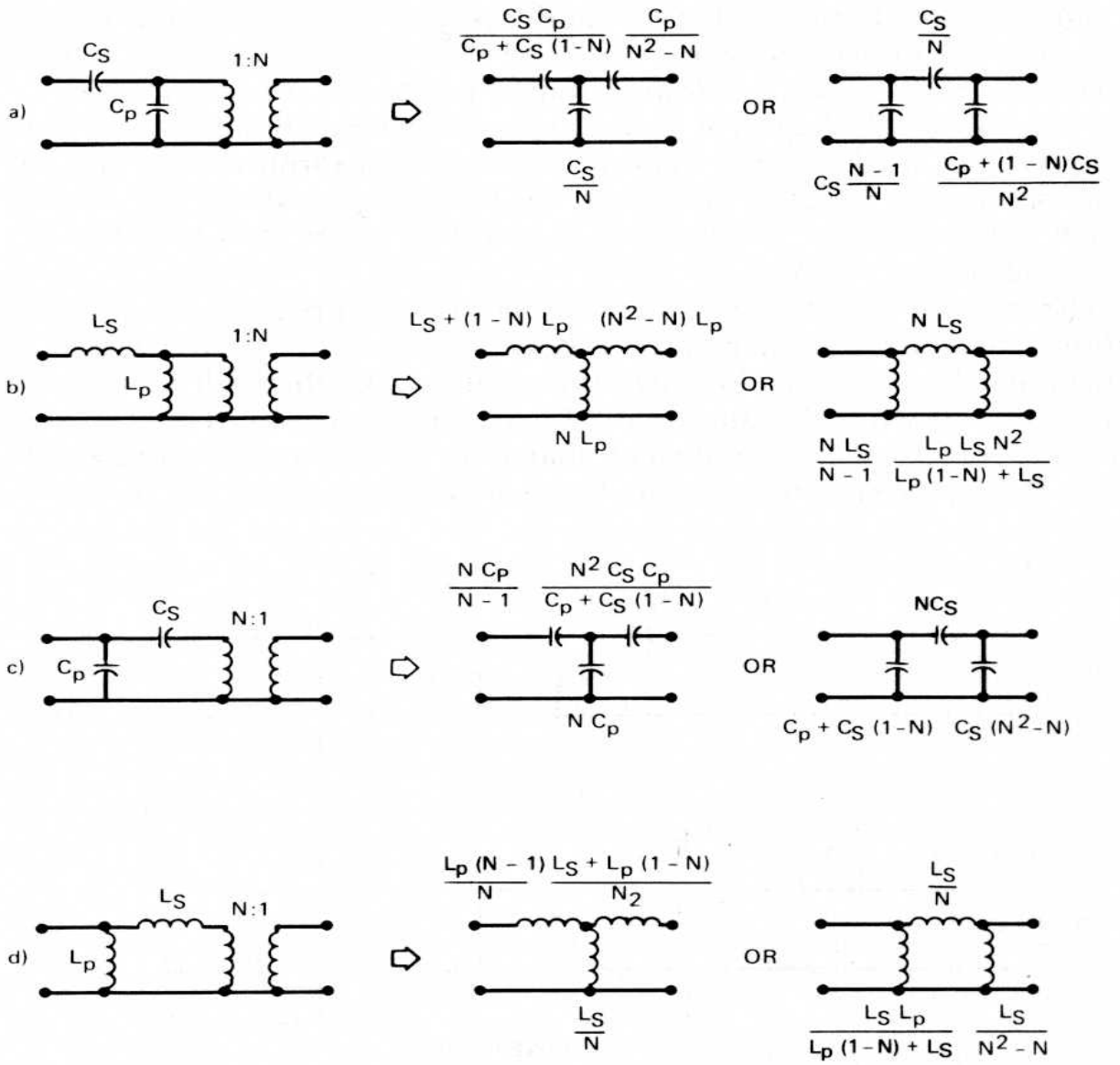

Figure 8.12 Norton transformer equivalents.

These equivalences are represented in Fig. 8.12. These are frequency-invariant representations. So, they are truly broadband equivalents, unlike the "J" or "K" inverters, which are sometimes used in narrow and moderate bandwidth filter designs.

The limit to the available transformer action must be considered. The maximum effective turns ratio is given by Eqs. (34) and (35). Attempts to go beyond this limit will result in negative elements in the T or pi equivalent circuits.

$$N_{\max} = \frac{C_S + C_P}{C_S} \tag{34}$$

$$N_{\max} = \frac{L_S + L_P}{L_P} \tag{35}$$

Since contiguous LP prototype elements yield pairs of inductors and capacitors in the BP network, it is useful to relate N_{max} to the relevant LP prototype elements ($g_i g_{i+1}$). This is expressed in

$$N_{max} = 1 + Q_T^2 g_i g_{i+1} \tag{36}$$

If one is willing to sacrifice some match performance in order to minimize the required number of network elements, Eq. (36) can be used. It is possible, by deviating from the Fano solution, to obtain adjacent LP prototype elements ($g_i g_{i+1}$) that simultaneously allow the necessary reactance absorption (g_1) and provide precisely the required N_{max} to complete the design. These bandpass forms are called minimum element [11] BP matching networks and are obtained by combining computer-aided synthesis with nonlinear programming.

Several practical BP matching network examples will be presented in Section 8.4.4.

8.4.2.2 Lowpass-to-Quasi-lowpass Transformation. Since practical microwave designs must behave as BP structures, it is natural also to seek LP or highpass (HP) configurations which behave as "pseudobandpass" structures. The HP and LP network forms of these pseudobandpass structures are often called quasi-highpass (QHP) and quasi-lowpass (QLP) networks. Varieties of frequency-variable transformations that address this need are available in the literature. Some provide the same network order in the transformed variable as in the LP domain, as in the work done by Christian and Eisenmann [12]. Perhaps the most well-known degree doubling QLP transformation was used by Matthaei [13] to form Chebyshev transformer networks. This work was later extended by Cottee and Joines [14] to permit prescribed reactance absorption, by allowing nonzero offset (flat-loss) in the response. The Butterworth QLP response approximation has also employed [15].

The QLP mapping will be considered in this section. It is illustrated in Fig. 8.13, and defined in Eq. (37), where S and p are the LP and QLP

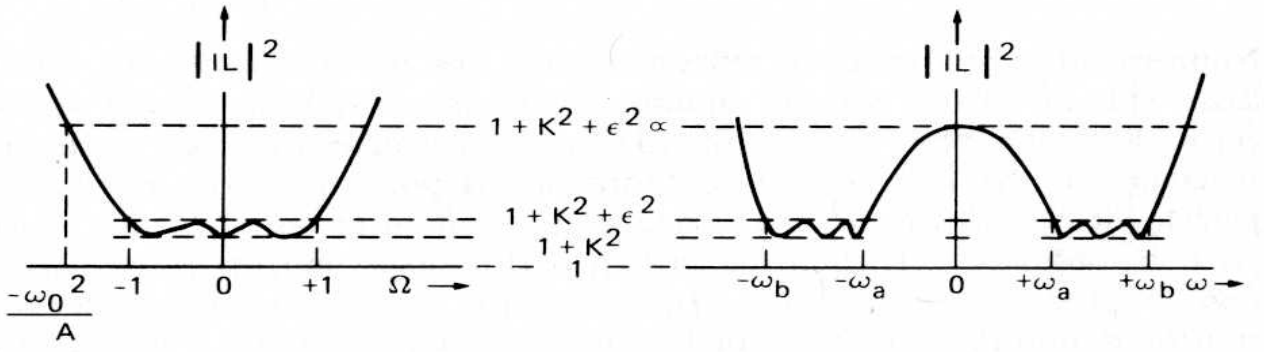

Figure 8.13 LP to QLP mapping.

complex frequencies, respectively. The band corner frequencies are f_1 and f_2.

$$S = \frac{-j(p^2 + \omega_0^2)}{A} \tag{37}$$

where

$$\omega_0^2 = \frac{\omega_a^2 + \omega_b^2}{2}, \qquad A = \frac{\omega_a^2 - \omega_b^2}{2},$$

$$\omega_a = \frac{2f_1}{f_2 + f_1}, \text{ and } \omega_b = \frac{2f_2}{f_2 + f_1}.$$

Reflection functions, pole and zero locations, and transfer functions can all be transformed to QLP form with Eq. (37). However, unlike BP mapping, network conversion on an element-by-element impedance basis is unsuccessful. Synthesis of this type of network can be accomplished by mapping LP reflection poles and zeros into QLP roots. The QLP reflection function can then be formed by expansion of the pole and zero factors. By Eq. (22), the driving-point impedance function can then be formed. Finally, the network is obtained from Eq. (22) by continued fractions. Denormalization is performed with respect to the low impedance port impedance and the arithmetic mean frequency, $(f_2 + f_1)/2$.

In the QLP synthesis procedure, just described, there was no step comparable to the Norton transformer insertion seen in BP design. How is the impedance transformation specified? The answer can be seen in Fig. 8.13, when the dc insertion loss is considered. Since, at dc, the resistive terminations are connected directly, the source-to-load impedance transformation can be controlled by adjusting the mismatch loss there. In so doing, a degree of freedom is lost. The response offset (flat loss) cannot be specified independently of the response ripple. As in Matthaei's case, with zero offset, a unique ripple solution was specified. As with Cottee and Joines, ripple and offset were constrained together uniquely to meet the design requirements. The linking relationship is given in Eq. (38), where r is the desired transformation ratio and N is the desired QLP network order:

$$\epsilon^2 = \left[\frac{(r-1)^2}{4r} - K^2\right] / \cosh^2\left\{2N \cosh^{-1}\left[\frac{\omega_0^2}{A}\right]\right\} \tag{38}$$

Nonzero offset is a result of reflection zeros that are not on the imaginary axis. This raises the issue of optimum placement (RHP or LHP) of the zeros. With this type of network, LHP zero placement provides maximum reactance at the low impedance (normalized) port. Similarly, RHP zero placement provides maximum reactance absorption at the high impedance port. In order to determine the match performance and necessary offset, Figs. 8.14–8.18 are provided. In each case, as a function of desired transformation ratio, several families of curves that are indexed by network order N and normalized bandwidth W are plotted. The vertical axis indicates

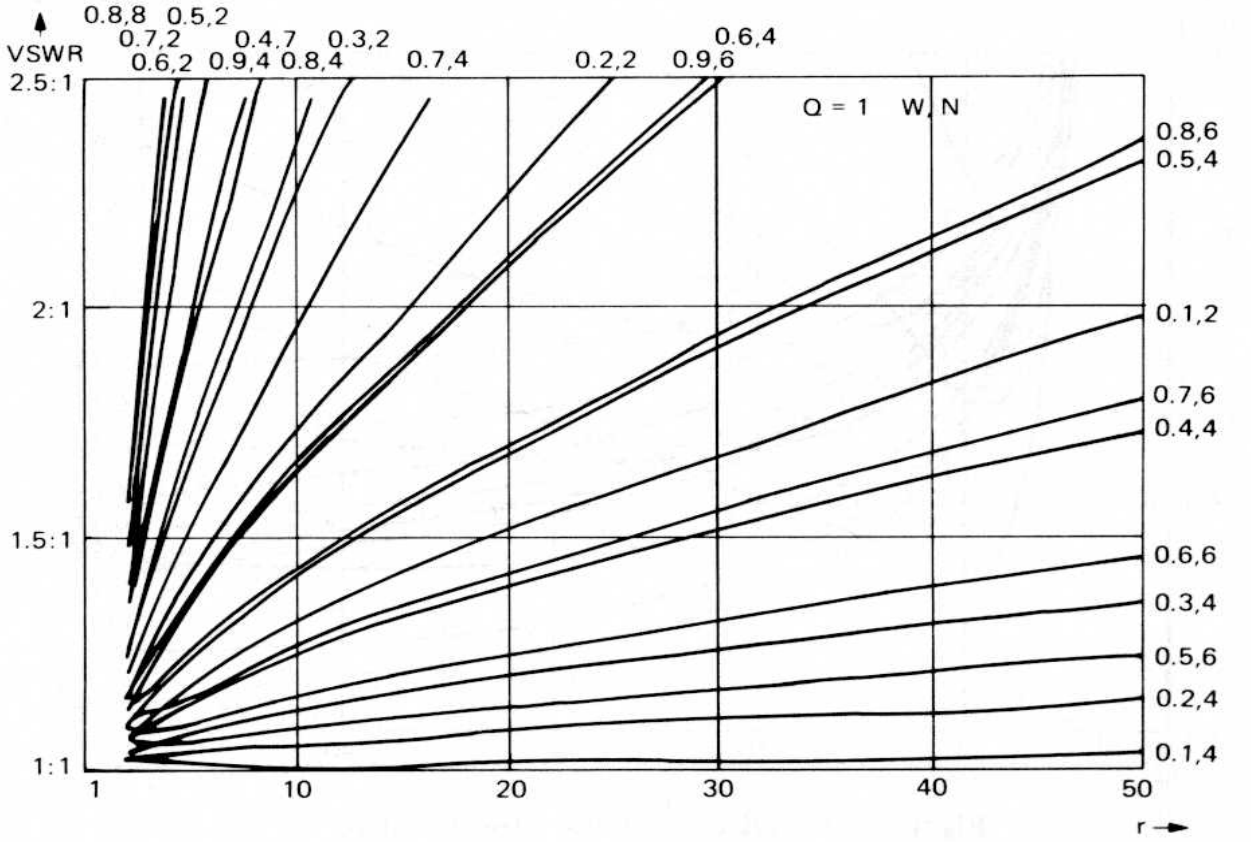

Figure 8.14 QLP reactance absorption, $Q = 1$.

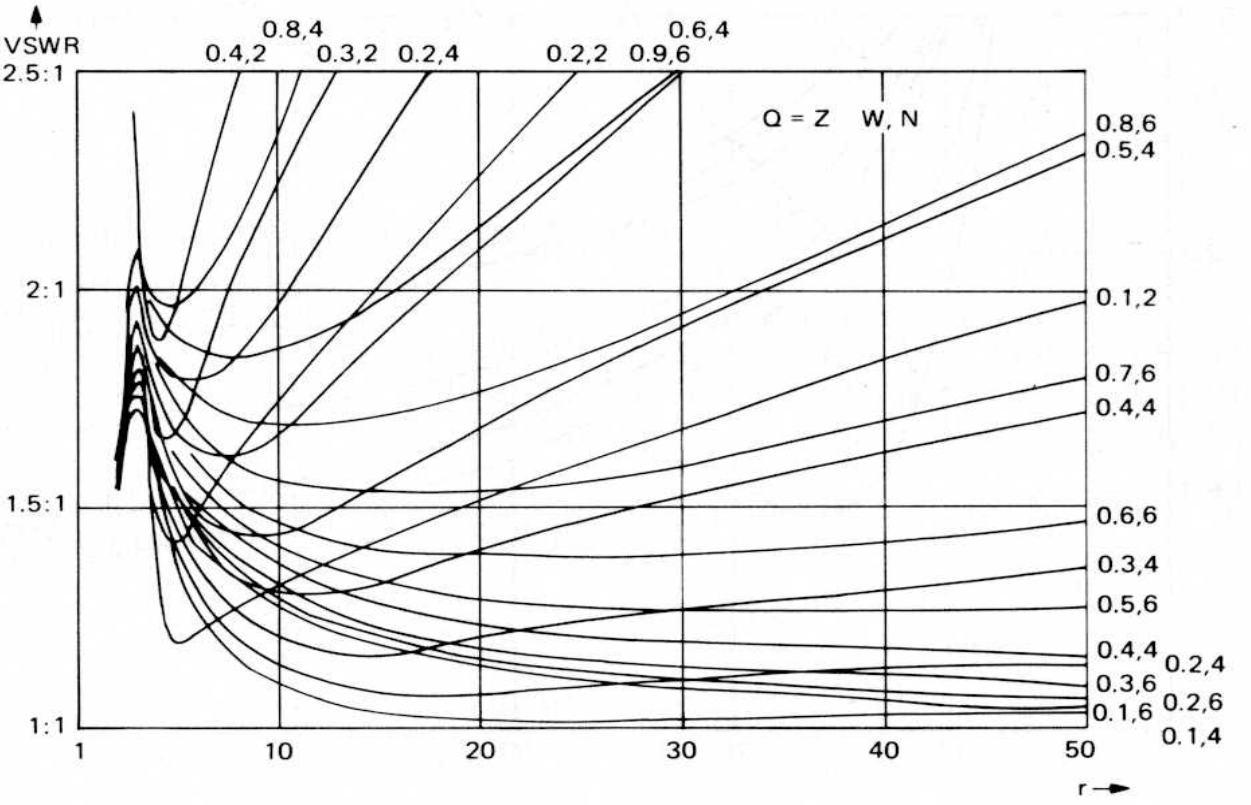

Figure 8.15 QLP reactance absorption, $Q = 2$.

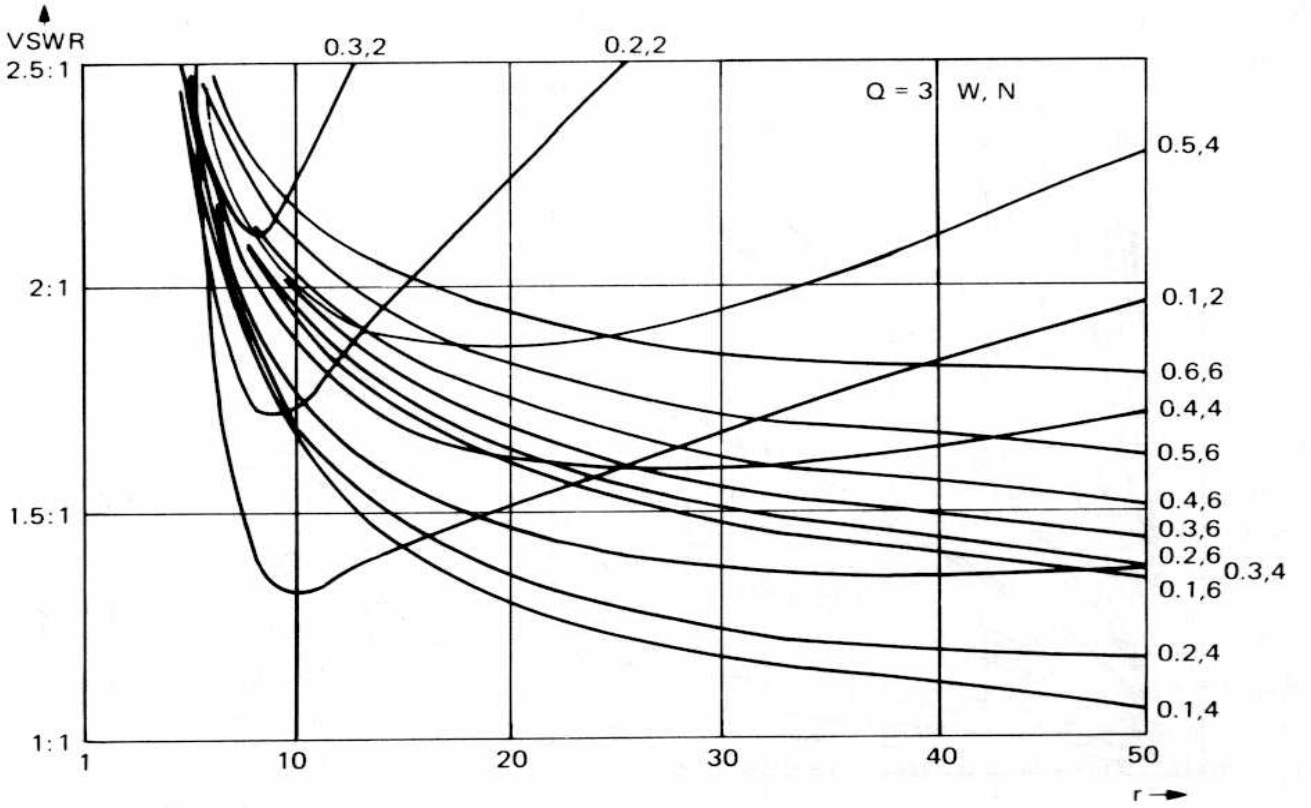

Figure 8.16 QLP reactance absorption, $Q = 3$.

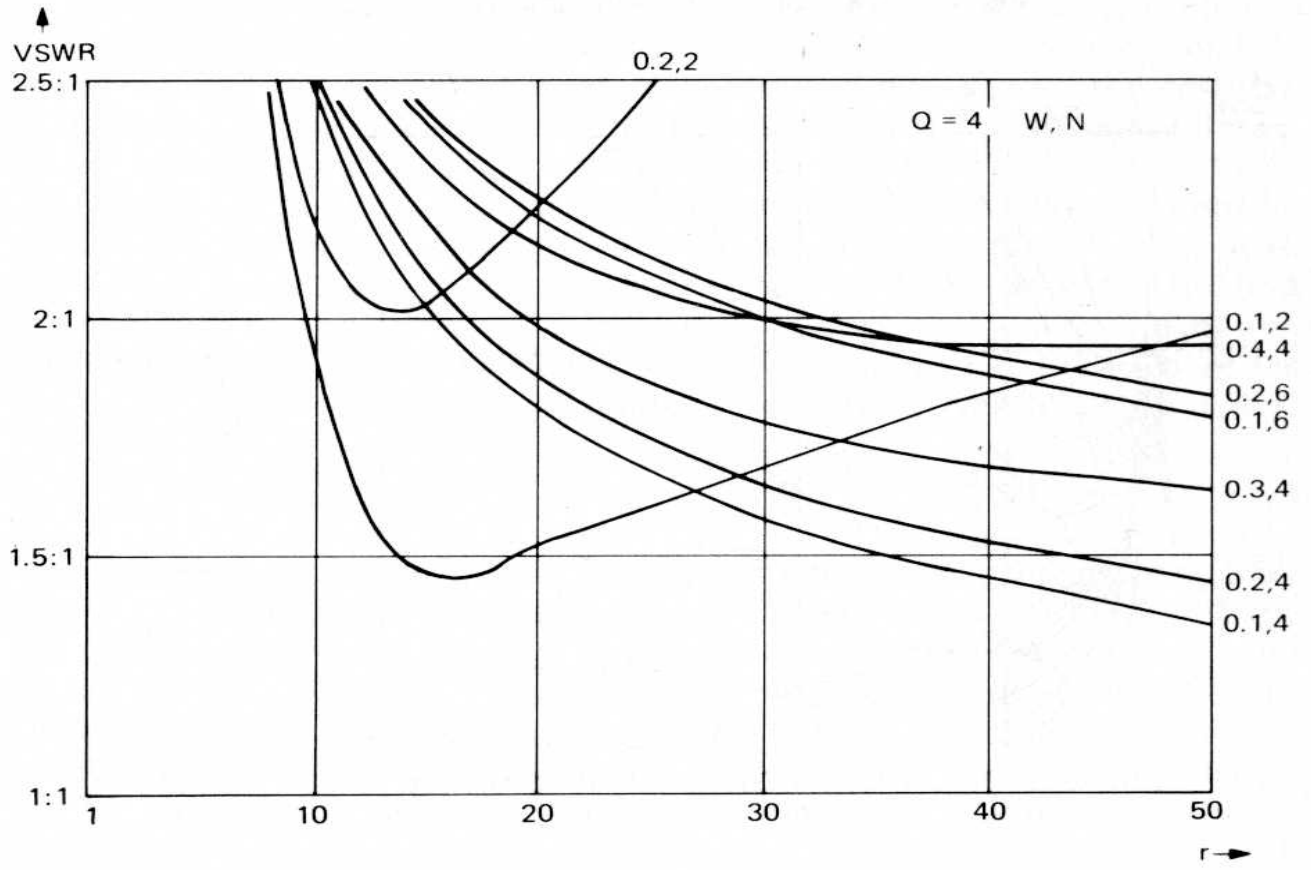

Figure 8.17 QLP reactance absorption, $Q = 4$.

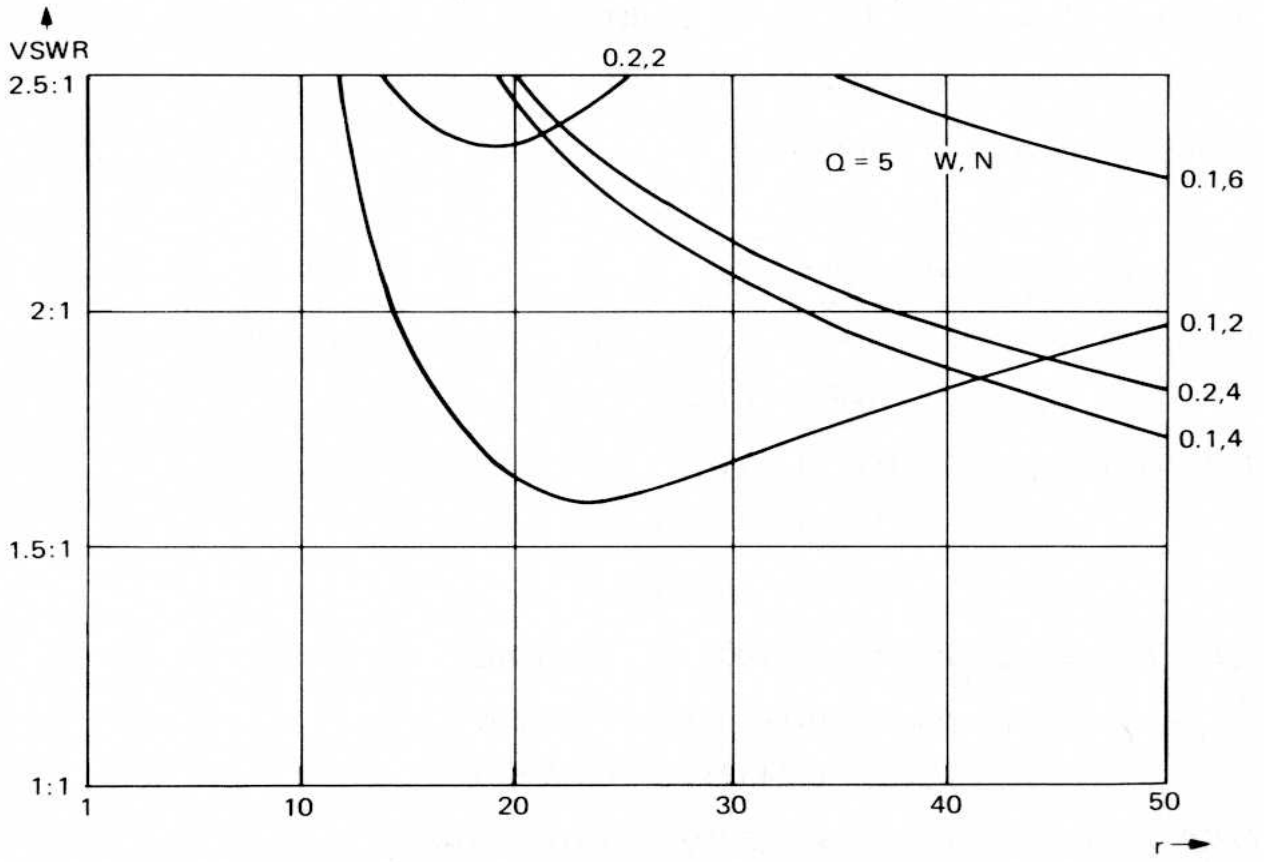

Figure 8.18 QLP reactance absorption, $Q = 5$.

the match performance. The normalized bandwidth is defined by

$$W = \frac{2(f_2 - f_1)}{f_2 + f_1} \tag{39}$$

A QUASI-LOWPASS MATCH EXAMPLE

Before moving on to QHP design, a QLP example is in order.

Suppose we wish to obtain an octave band match from 4 GHz to 8 GHz into a series load that is comprised of a 0.132 nH inductor and a 2.0 Ω resistor. Use a sixth-order matching network. A 50 Ω source is given. So, $r = 25$.

Match Limits:
$$Q_{\text{QLP}} = \frac{(2\pi 6)(10^9)(0.132\text{ nH})(10^{-9})}{2.0\ \Omega} = 2.5$$

$$Q_{\text{Bode}} = (Q_{\text{QLP}})(W) = (2.5)(0.667) = 1.667$$

$$\rho_{\text{Bode}} = \exp\left(\frac{-\pi}{1.667}\right) = 0.152$$

$$\text{VSWR}_{\text{Bode}} = 1.34{:}1$$

$$\text{VSWR}_{\text{max}} = 1.7{:}1 \text{ (from Figs. 8.15 and 8.16)}$$

Response Parameters: Offset = 0.19 dB

Ripple= 0.13 dB

Fano Parameters: $a = 0.818$

$b = 0.339$

LP Poles: $S_{p1} = -0.912815 + j\,0$

$S_{p2} = -0.456408 + j\,1.172571$

$S_{p3} = -0.456408 - j\,1.172571$

LP Zeros: $S_{z1} = -0.351723 + j\,0$

$S_{z2} = -0.172586 + j\,0.916165$

$S_{z3} = -0.172586 - j\,0.916165$

QLP Poles: $p_{p1},\ p_{p1}^* = -0.279045 \pm j\,1.090402$

$p_{p2},\ p_{p2}^* = -0.110227 \pm j\,1.380208$

$p_{p3},\ p_{p3}^* = -0.243953 \pm j\,0.623627$

QLP Zeros: $P_{z1},\ p_{z1}^* = -0.108579 \pm j\,1.059670$

$P_{z2},\ p_{z2}^* = -0.043817 \pm j\,1.312939$

$P_{z3},\ p_{z3}^* = -0.080805 \pm j\,0.711944$

$$\rho = \frac{p^6 + 0.4664p^5 + 3.4421p^4 + 1.0960p^3 + 3.5131p^2 + 0.5599p + 1.0053}{p^6 + 1.2665p^5 + 4.1353p^4 + 3.3118p^3 + 4.5699p^2 + 1.7900p + 1.0891}$$

$$\frac{Z_{dp}}{R_0} = \frac{2p^6 + 1.7329p^5 + 7.5774p^4 + 4.4079p^3 + 8.0830p^2 + 2.3500p + 2.0944}{0.800p^5 + 0.6932p^4 + 2.2160p^3 + 1.057p^2 + 1.2300p + 0.08378}$$

QLP Prototype: $g_0 = 1.0\ \Omega$

$g_1 = 2.5$ H

$g_2 = 0.3925$ F

$g_3 = 8.1518$ H

$g_4 = 0.1486$ F

$g_5 = 17.3982$ H

$g_6 = 0.04617$ F

$g_7 = 25.00\ \Omega$

Denormalized QLP Prototype: Frequency scale by $2\pi 6(10^9)$

Impedance scale by 2.0

REFLECTION ZERO PLACEMENT: LHP, LHP, LHP

BANDWIDTH = 66.66 %
LOWER STOPBAND LOSS = 8.2994 dB
OFFSET = 0.192 dB, RIPPLES = 0.128 dB
PASSBAND MAXIMUM LOSS = 0.3192 dB
PASSBAND VSWR (RIPPLE + OFFSET) = 1.725 : 1

QUASI-LOWPASS MATCH

R = 2	Ohm
L = 0.132	NANO-HENRY
C = 5.206	PICO-FARAD
L = 0.432	NANO-HENRY
C = 1.971	PICO-FARAD
L = 0.923	NANO-HENRY
C = 0.612	PICO-FARAD
R = 50	Ohm

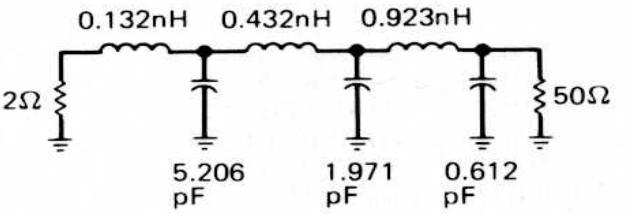

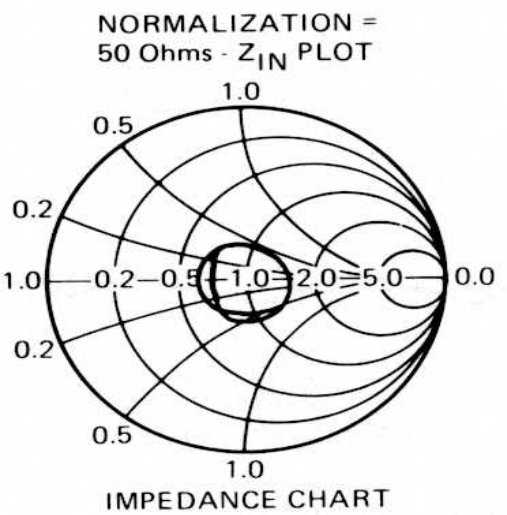

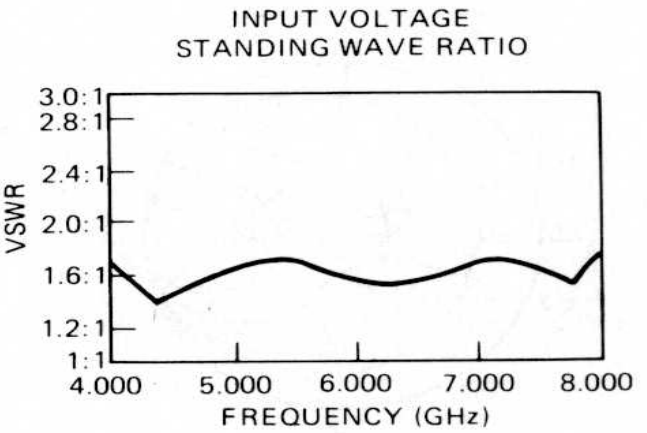

Figure 8.19 QLP match example: LHP zeros.

Hence, the QLP matching network shown in Fig. 8.19 is obtained:

$$\begin{aligned}
&(\text{From } g_0) && R_L = 2.000\,\Omega \\
&(\text{From } g_1) && L_1 = 0.132\,\text{nH} \\
&(\text{From } g_2) && C_1 = 5.206\,\text{pF} \\
&(\text{From } g_3) && L_2 = 0.432\,\text{nH} \\
&(\text{From } g_4) && C_2 = 1.971\,\text{pF} \\
&(\text{From } g_5) && L_3 = 0.932\,\text{nH} \\
&(\text{From } g_6) && C_3 = 0.612\,\text{pF} \\
&(\text{From } g_7) && R_s = 50.00\,\Omega
\end{aligned}$$

REFLECTION ZERO PLACEMENT: RHP, RHP, RHP

BANDWIDTH = 66.66 %
LOWER STOPBAND LOSS = 8.2994 dB
OFFSET = 0.192 dB, RIPPLES = 0.128 dB
PASSBAND MAXIMUM LOSS = 0.3192 dB
PASSBAND VSWR (RIPPLE + OFFSET) = 1.725 : 1

QUASI-LOWPASS MATCH

R = 2	Ohm
L = 0.061	NANO-HENRY
C = 9.23	PICO-FARAD
L = 0.197	NANO-HENRY
C = 4.324	PICO-FARAD
L = 0.52	NANO-HENRY
C = 1.326	PICO-FARAD
R = 50	Ohm

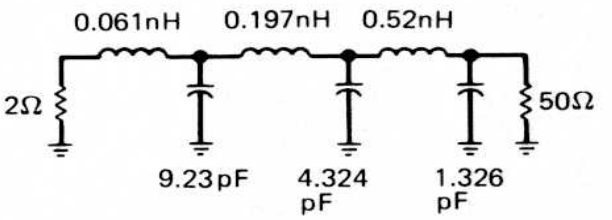

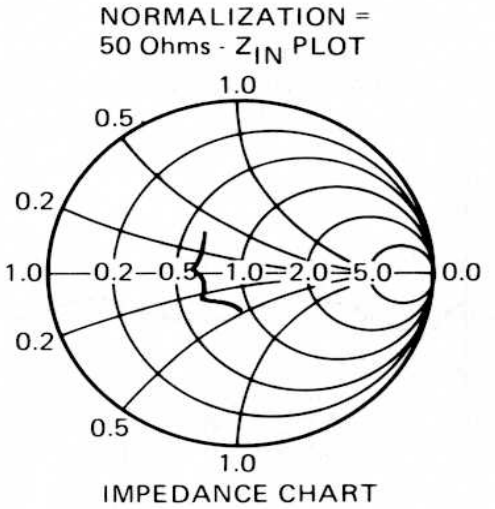

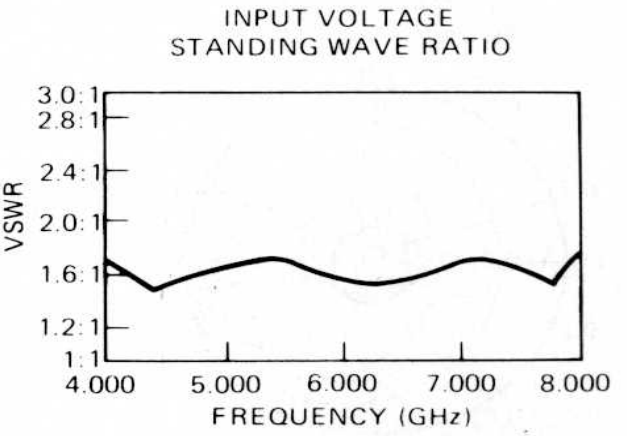

Figure 8.20 QLP match example: RHP zeros.

Note that the desired load model was forced. This occurred through the selection of the Fano parameters and LHP zero placement. If all reflection zeros are symmetrically moved to the RHP, the QLP network in Fig. 8.20 is obtained. Note that the mismatch magnitude performance is identical, but the input port capacitor has doubled and the output port inductor has correspondingly reduced in size! For comparison, consider the Matthaei zero offset QLP network, which results from the same requirements except for prescribed reactance absorption. This case, shown in Fig. 8.21, results when reflection zeros are placed on the imaginary axis. Note that the size of the reactive elements at each port falls between the RHP and LHP cases.

8.4.2.3 Lowpass to Quasi-Highpass Transformation. A pseudobandpass alternative to the QLP is the quasi-highpass (QHP) network. Since realization of QHP designs is quite similar to that of the QLP, this section will be brief.

BANDWIDTH = 66.66 %
LOWER STOPBAND LOSS = 8.2994 dB
PASSBAND RIPPLE LOSS = 0.1347 dB
PASSBAND RIPPLE VSWR = 1.423 : 1

QUASI-LOWPASS MATCH

R = 2	Ohm
L = 0.084	NANO-HENRY
C = 7.42	PICO-FARAD
L = 0.29	NANO-HENRY
C = 2.9	PICO-FARAD
L = 0.742	NANO-HENRY
C = 0.849	PICO-FARAD
R = 50	Ohm

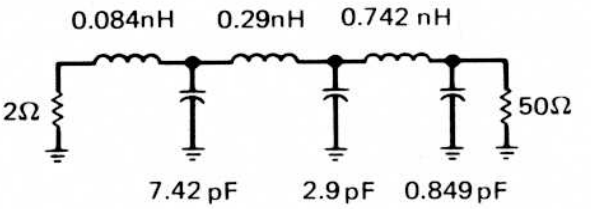

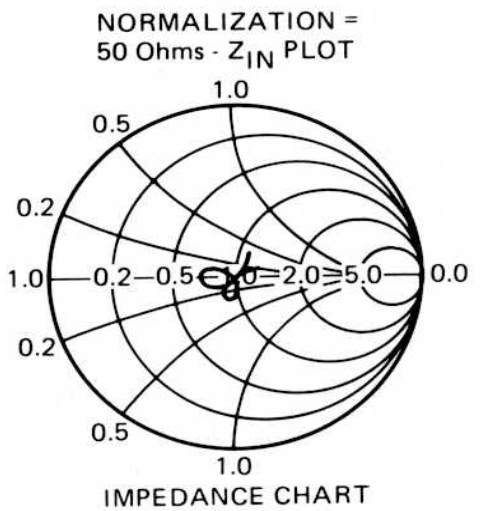

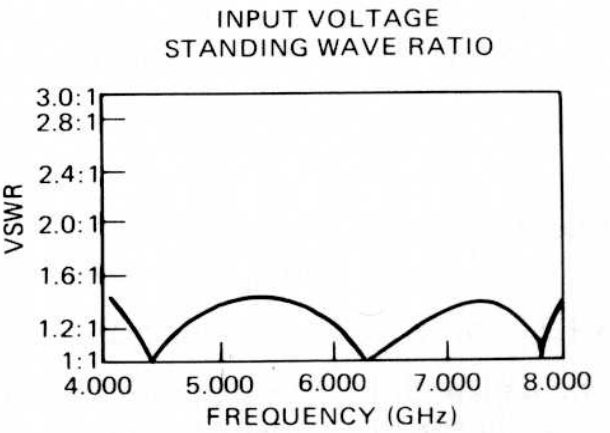

Figure 8.21 QLP match example: no offset.

The QHP mapping to be considered in this section is illustrated in Fig. 22, and defined in Eq. (40), where S and p are the LP and QHP complex frequencies, respectively. The band corner frequencies are f_1 and f_2.

$$S = -j\left[\frac{(\omega_1\omega_2)^2}{Ap^2} + \frac{\omega_0^2}{A}\right] \tag{40}$$

where $\omega_0^2 = \dfrac{\omega_a^2 + \omega_b^2}{2}$, $\quad A = \dfrac{(\omega_a^2 - \omega_b^2)}{2}$,

$\omega_a = \dfrac{2f_1}{f_2 + f_1}$, and $\omega_b = \dfrac{2f_2}{f_2 + f_1}$.

Like Eq. (37), Eq. (40) does not allow network conversion on an element-by-element impedance basis. However, element-by-element conversion from QLP to QHP can be accomplished with Eq. (41), where P and S are

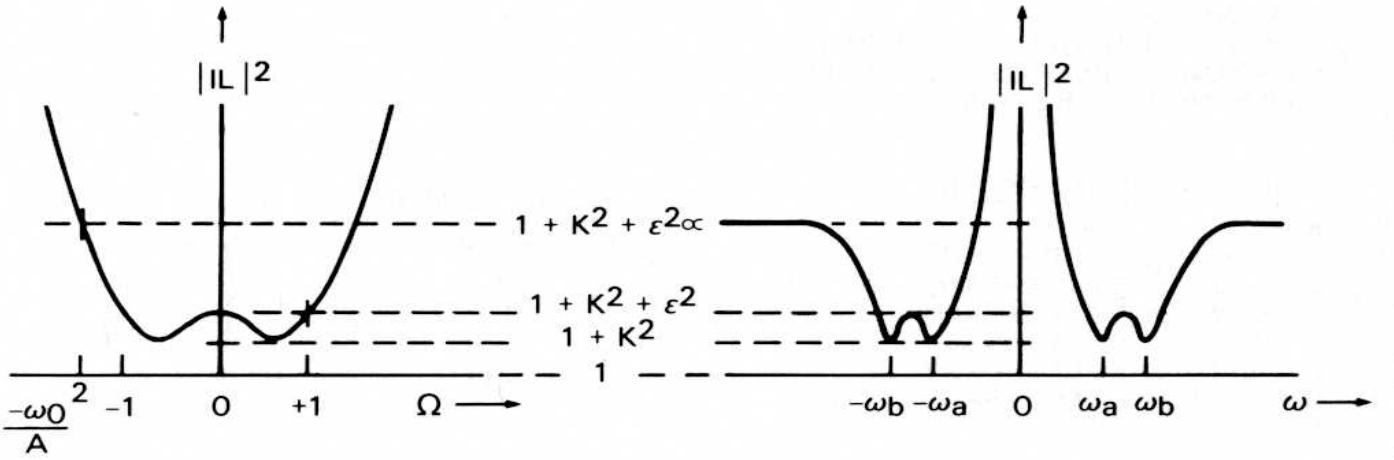

Figure 8.22 LP to QHP mapping.

the QLP and QHP complex frequencies, respectively. Synthesis of this type of network can be accomplished in a manner identical to that of the QLP.

$$P = \frac{\omega_1 \omega_2}{S} \tag{41}$$

where $\omega_1 = 2\pi f_1$, and $\omega_2 = 2\pi f_2$.

8.4.3 One-port Load Modeling

The unilateral FET model, previously discussed in Section 8.2, represents an embodiment of two simple one-port impedance models. It is well known that intrinsic device impedance behavior can be accurately represented in this manner. However, when feedback or lossy branch gain equalization is employed, a single *RC* section is an inadequate representation. Sometimes nonunilateral behavior can be strong enough to require a more sophisticated model. Recently, Mellor [16] has derived closed-form expressions for second-order LP and HP one-port impedance models. Second- and fourth-order closed-form BP models have been used successfully by this author [17] for many years. This modeling technique will now be discussed. When the occasional need arises for higher-order models, this method can be easily extended to cover those cases.

In order to provide a form that is compatible with the subsequent synthesis step, all one-port models are required to be two-port LC networks that are resistively terminated. The two topologies that will be considered are illustrated in Fig. 8.23. Each reactance or susceptance block is allowed up to second-order behavior. So, fourth-order models can thereby be realized. To avoid Matthaei's "situation 2," the innermost branch of the model must provide the dominant behavior. The outermost branch provides a perturbational contribution. Therefore, the two forms to be considered can be seen in Fig. 8.24.

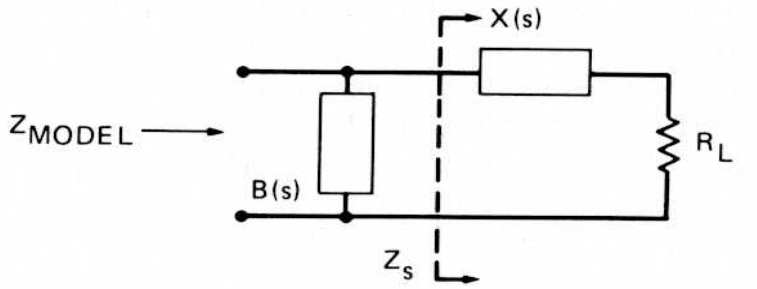

(a) SERIES BEHAVIOR WITH SHUNT PERTURBATION

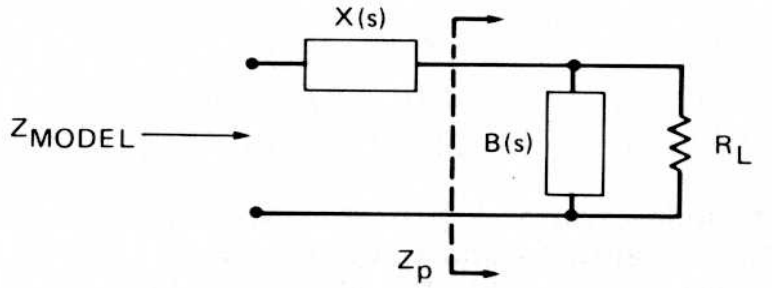

(b) SHUNT BEHAVIOR WITH SERIES PERTURBATION

Figure 8.23 One-port model topologies.

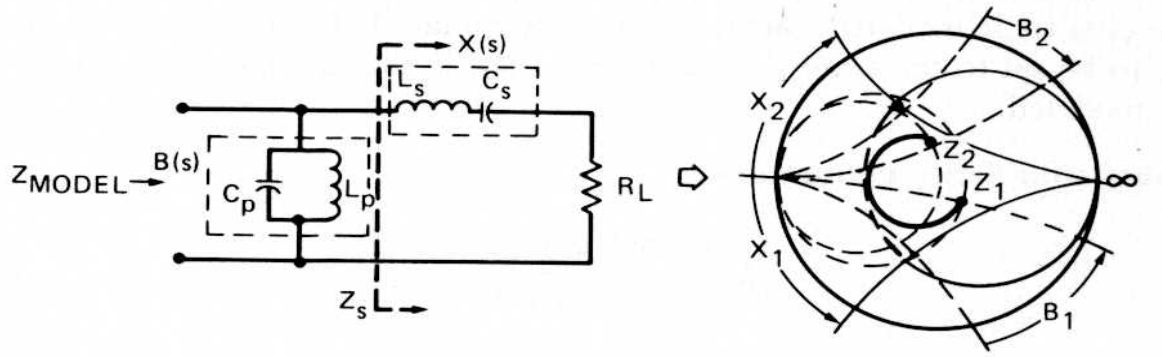

(a) SERIES BEHAVIOR WITH SHUNT PERTURBATION

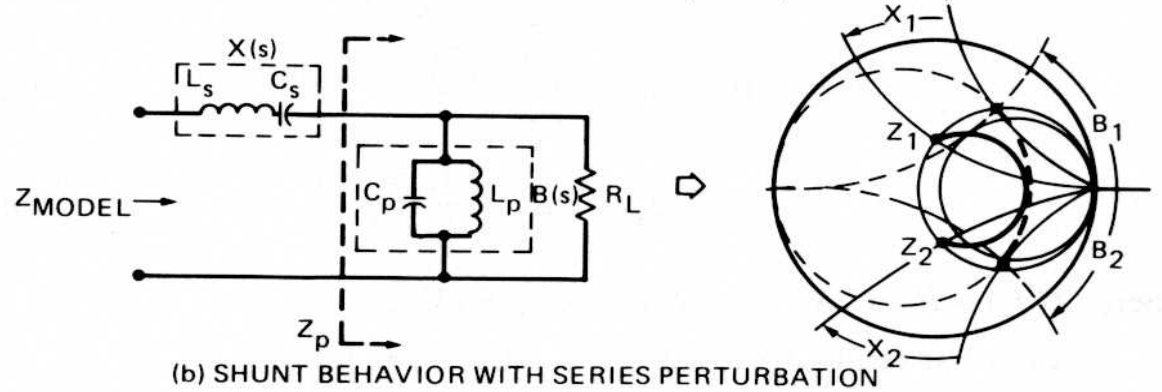

(b) SHUNT BEHAVIOR WITH SERIES PERTURBATION

Figure 8.24 Fourth-order models.

The LC values in the second-order subsections can be determined from the reactance (series case) or susceptance levels at the band corners, f_1 and f_2. These calculations, which result from simultaneously solving two equations in two unknowns, are given in Eqs. (42–45). The reactance and susceptance levels at f_1 and f_2 are X_1, X_2, B_1 and B_2, respectively.

$$L_S = \frac{f_2 X_2 - f_1 X_1}{2\pi(f_2^2 - f_1^2)} \tag{42}$$

$$C_S = \frac{f_2^2 - f_1^2}{2\pi(f_1^2 f_2 X_2 - f_1 f_2^2 X_1)} \tag{43}$$

$$L_P = \frac{f_2^2 - f_1^2}{2\pi(f_1^2 f_2 B_2 - f_1 f_2^2 B_1)} \tag{44}$$

$$C_P = \frac{f_2 B_2 - f_1 B_1}{2\pi(f_2^2 - f_1^2)} \tag{45}$$

The fourth-order models seen in Fig. 8.24 are obtained by a decomposition into second-order subnetworks and solution of Eqs. (42–45). To see this decomposition, consider Fig. 8.25. The closed-form solution for the reactance and susceptance shifts (X_1, X_2, B_1, and B_2) are given in Eqs. (46–53). Since the end points of the locus are fixed, the value of the terminal resistance adjusts the amount of curvature. For series-dominant behavior, R_L is usually set to the lowest value that is encountered in the real part of the data to be modeled. Similarly, shunt-dominant behavior usually requires R_L to be set to the largest value encountered in the real part of the data to be modeled.

Shunt with Series Perturbation

$$B_1 = \frac{A\sqrt{[R_L/R_A - 1]}}{R_L} \tag{46}$$

$$X_1 = X_A + AR_A\sqrt{\frac{R_L}{R_A - 1}} \tag{47}$$

$$B_2 = \frac{B\sqrt{[R_L/R_B - 1]}}{R_L} \tag{48}$$

$$X_2 = X_B + BR_B\sqrt{\frac{R_L}{R_B - 1}} \tag{49}$$

where $Z(f_1) = R_A + jX_A$, $\quad Z(F_2) = R_B + jX_B$,

$A = +1$ if $\text{Imag}\{Z_p(f_1)\} \le 0$, $\quad A = -1$ if $\text{Imag}\{Z_p(f_1)\} > 0$,

$B = +1$ if $\text{Imag}\{Z_p(f_2)\} \le 0$, and $B = -1$ if $\text{Imag}\{Z_p(f_2)\} > 0$.

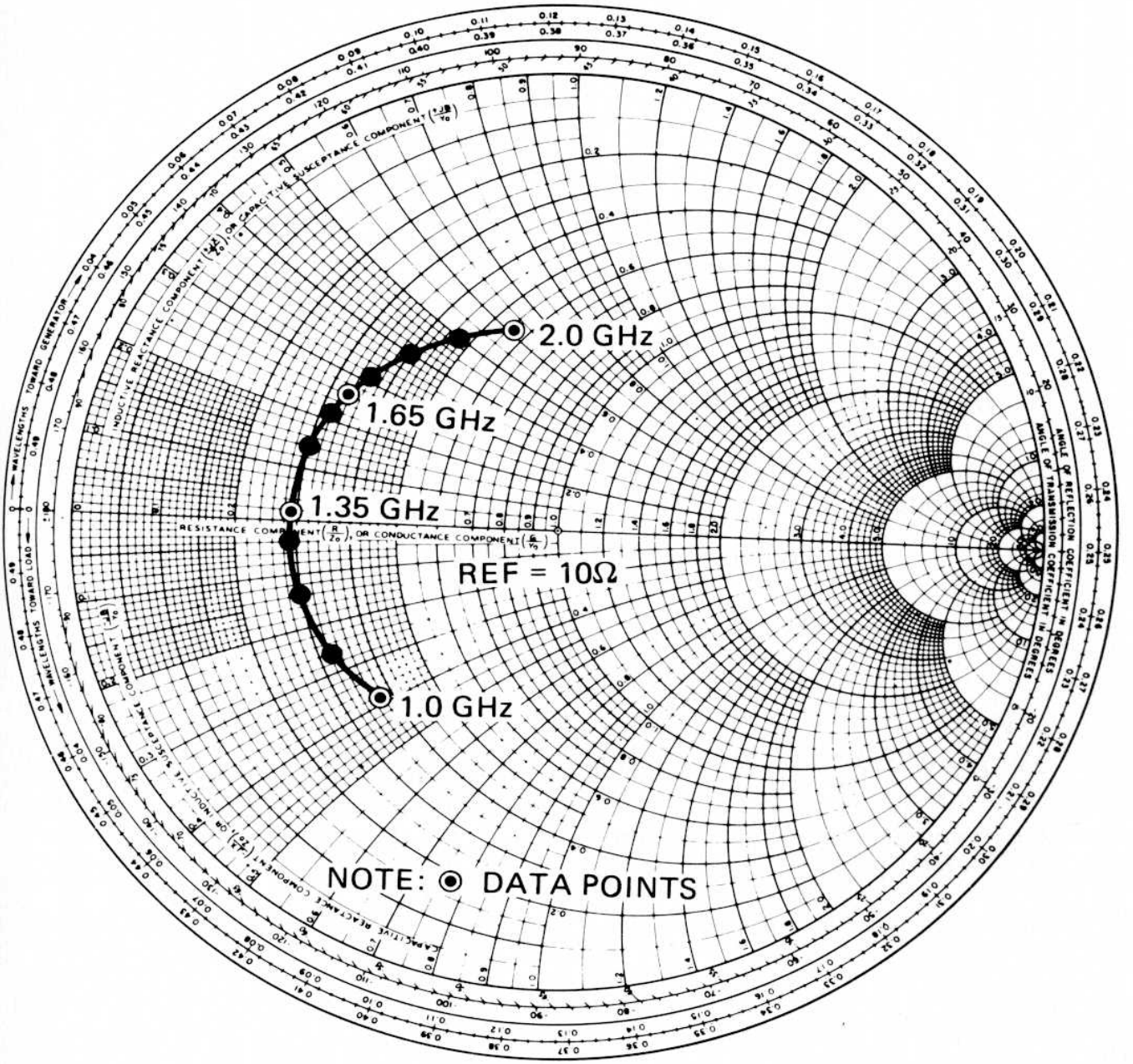

Figure 8.25 Impedance data to be modeled.

Series with Shunt Perturbation

$$X_1 = AR_L\sqrt{\frac{R_A(1+Q_1^2)}{R_L-1}} \tag{50}$$

$$B_1 = \frac{A\sqrt{[R_A(1+Q_1^2)/R_L-1]}}{R_A(1+Q_1^2)} - \frac{Q_1^2}{X_A(1+Q_1^2)} \tag{51}$$

$$X_2 = BR_L\sqrt{\frac{R_B(1+Q_2^2)}{R_L-1}} \tag{52}$$

$$B_2 = \frac{B\sqrt{[R_B(1+Q_2^2)/R_L-1]}}{R_B(1+Q_2^2)} - \frac{Q_2^2}{X_B(1+Q_2^2)} \tag{53}$$

where $Z(f_1) = R_A + jX_A$, $Z(f_2) = R_B + jX_B$,

$$Q_1 = \frac{|X_A|}{R_A}, \qquad Q_2 = \frac{|X_B|}{R_B},$$

$A = -1$ if $\text{Imag}\{Z_S(f_1)\} \le 0$, $A = +1$ if $\text{Imag}\{Z_S(f_1)\} > 0$,

$B = -1$ if $\text{Imag}\{Z_S(f_2)\} \le 0$, and $B = - + 1$ if $\text{Imag}\{Z_S(f_2)\} > 0$.

A LOAD MODEL EXAMPLE

As a numerical example, we will model the following data with a fourth-order model:

Frequency (GHz)	R_{Load}	X_{Load}
1.00	4.0	−4.0
1.35	3.0	0.0
1.65	3.5	3.0
2.00	6.0	7.0

As seen in Fig. 8.25, the behavior to be modeled is predominantly series-resonant. So, we choose the series model with the shunt perturbation. Since the minimum value seen in the real part of the data is 3.0 Ω, we set $R_L = 3.0\,\Omega$. From Eqs. (50–53), we obtain

$$X_1 = -3.873$$

$$B_1 = -0.0364$$

$$X_2 = 5.788$$

$$B_2 = 0.0538$$

The LC element values within the model are then obtained from Eqs. (42–45). The model and modeled results can be seen in Fig. 8.26.

8.4.4 A Two-stage Power Amplifier Design Example

In this section, we will put to use the circuit design procedures that have been detailed in the previous sections of this chapter. As an illustrative

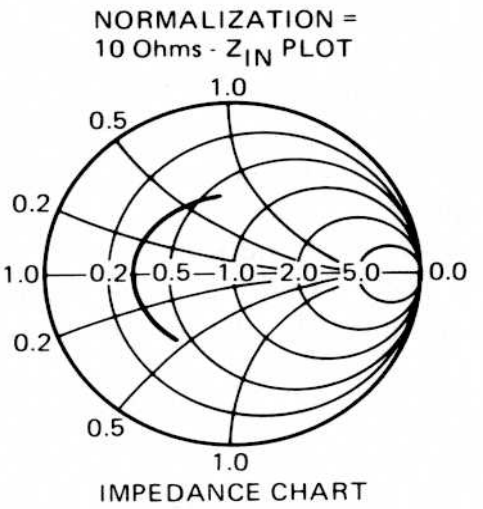

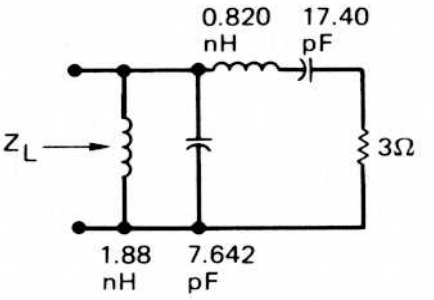

FREQ (MHz)	R_{IN}	X_{IN}
1000	4.04	-4.16
1100	3.40	-2.57
1200	3.11	-1.35
1300	3.00	-0.32
1400	3.02	0.62
1500	3.15	1.52
1600	3.37	2.43
1700	3.72	3.38
1800	4.21	4.42
1900	4.92	5.58
2000	5.93	6.89

Figure 8.26 Load model example results.

vehicle, we will design a two-stage $\frac{1}{2}$ W amplifier for operation between 8 and 12 GHz. Therefore, three matching network designs are required. The FET model that will serve as a basis for this example is the Hughes TRC-4080. This is an *X*-band geometry with a gate length of 0.8 μm. The large-signal unilateral model for a total gate width of 1 mm is given in Fig. 8.27. Similarly, a 330 μm driver device model is shown as a 3:1 impedance scaling.

The output port impedance behavior of this model represents the complex conjugate of the optimum power load, rather than the FET source impedance strictly. This is because the optimum power match impedance

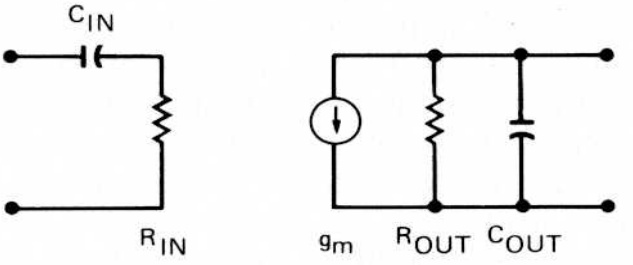

GATE WIDTH (MICRON)	$R_{IN}(\Omega)$	C_{IN}(pF)	g_m(℧)	$R_{OUT}(\Omega)$	C_{OUT}(pF)
1000	2.4	1.28	0.073	54.	0.34
330	7.2	0.427	0.024	165.	0.114

Figure 8.27 FET one-port impedance models.

requirements differ from small-signal reflection match requirements. When a network is designed to provide an impedance match with this model, that network will also provide an optimum power load for the FET. From this example, it should now be apparent that any desired impedance behavior can be approximated by modeling its complex conjugate and designing a matching network to interface with that model.

The first step in this example is to make an assessment of the device Q's and corresponding match performance in the 8–12 GHz band. Fano networks are used in this example; thus, midband is the geometric center.

$$f_0 = \sqrt{(8\text{ GHz})(12\text{ GHz})} \qquad = 9.798\text{ GHz} \tag{64}$$

$$Q_T = \frac{9.798\text{ GHz}}{12\text{ GHz} - 8\text{ GHz}} \qquad = 2.44949 \tag{55}$$

$$Q_{In} = \frac{1}{(2\pi 9.798)(10^9)(1.28)(10^{-12})(2.4)} = 5.2877 \tag{56}$$

$$Q_{Out} = (2\pi 9.798)(10^9)(0.34)(10^{-12})(54) \quad = 1.1635 \tag{57}$$

From these Q's we can calculate the Bode match limits. To do this, the bandpass Q must transformed into its equivalent LP Q with Eq. (58):

$$Q_{LP} = \frac{Q_{BP}}{Q_T} \tag{58}$$

$$|\rho|_{\text{Bode-in}} = \exp\left(\frac{-\pi 2.4495}{5.2877}\right) = 0.233 \tag{59}$$

$$|\rho|_{\text{Bode-out}} = \exp\left(\frac{-\pi 2.4495}{1.1635}\right) = 0.0013 \tag{60}$$

Clearly, the output match performance appears to be quite good. From (59), the input performance does not look attractive. However, since microwave FET devices exhibit −6 dB/octave roll-off in $|S_{21}|$ with increasing frequency, some form of amplitude equalization is required. This could be achieved by feedback, lossy branch compensation, or controlled mismatch. For superior power amplifier performance, feedback and controlled mismatch are rejected due to output power loss and high reflection, respectively. Lossy compensation of the input port can most conveniently be applied with a shunt RLC branch. The excess available device gain at lower frequencies can be compensated for by applying the proper LC reactance slope. From gain-bandwidth considerations (Bode), we should not be surprised to find that the resultant gain compensated match performance has improved. Another way of looking at this is as a frequency tailored input "de-Qing." Figure 8.28 shows the compensated input models. When these one ports are reflection-matched, a properly gain-compensated amplifier will

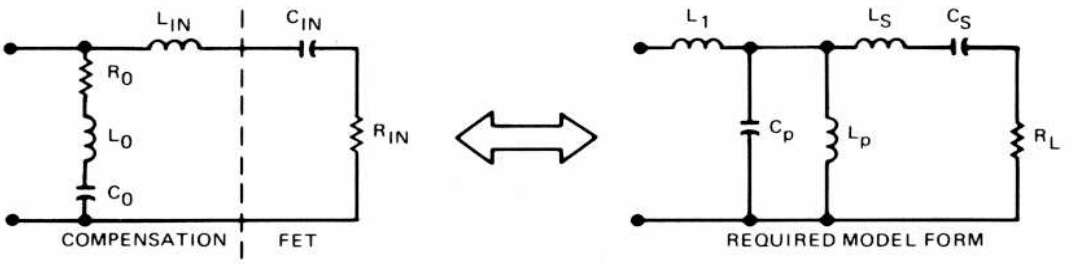

GATE WIDTH	R_{IN}	C_{IN}	L_{IN}	R_0	L_0	C_0	L_1	C_p	L_p	C_S	L_S	R_L
1000 MICRON	2.4Ω	1.28pF	0.137nH	21Ω	0.25nH	3.0pF	-0.0516nH	0.251pF	0.274nH	1.597pF	0.167nH	2.851Ω
330 MICRON	7.2Ω	0.427pF	0.412nH	65Ω	0.75nH	1.0pF	-0.1549nH	0.0843pF	0.822nH	0.523pF	0.501nH	8.55Ω

Figure 8.28 Lossy branch compensation input models.

result. For matching network design by the techniques already discussed, these compensated input ports must be remodeled into a proper form: an *LC* two-port that is terminated with a single resistor. These alternative representations are also illustrated in Fig. 8.28. As a result, the input BP Q is 3.588. The corresponding Bode match reflection limit is now 0.117.

The input, interstage, and output matching networks can now be designed. A sixth-order network (including the model absorbed) will be used at the amplifier input. At the interstage, an eight-order model is needed. And due to the relatively low-output Q, only a fourth-order output matching network is required.

Input Match

$$N = 6$$

$$Q_{\text{Load}} = 3.588$$

$$a = 0.882$$

$$b = 0.313$$

$$\text{VSWR}_{\text{Bode}} = 1.27{:}1$$

$$\text{VSWR}_{\text{max}} = 1.53{:}1$$

$$\text{VSWR}_{\text{min}} = 1.37{:}1$$

$$g_0 = 1.0$$

$$g_1 = 1.465$$

$$g_2 = 0.890$$

$$g_3 = 1.036$$

$$g_4 = 0.733$$

The bandpass transformed input matching network is depicted in Fig. 8.29a. An inductive Norton transformer is then inserted to obtain the 50 Ω input port (Fig. 8.29b). Input match performance is shown in Fig. 8.29c.

Interstage Match

$$N = 8$$

$$Q_{\text{Source}} = 1.164$$

$$Q_{\text{Load}} = 3.588$$

$$a = 0.928$$

$$b = 0.521$$

$$\text{VSWR}_{\text{max}} = 1.50{:}1$$

$$\text{VSWR}_{\text{min}} = 1.48{:}1$$

$$g_0 = 1.0$$

$$g_1 = 1.465$$

$$g_2 = 0.867$$

$$g_3 = 1.617$$

$$g_4 = 0.317$$

$$g_5 = 1.497$$

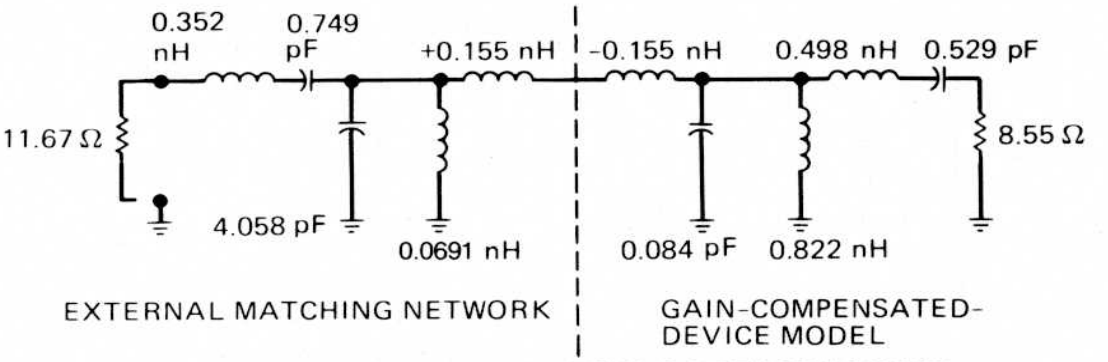

a) BP TRANSFORMED INPUT MATCHING NETWORK/MODEL

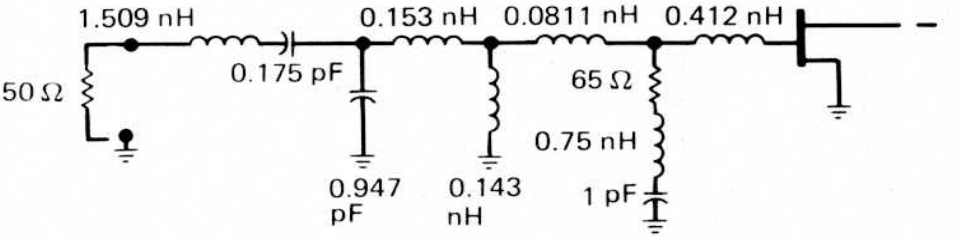

b) COMPLETED INPUT NETWORK, AFTER NORTON TRANSFORMER INSERTION

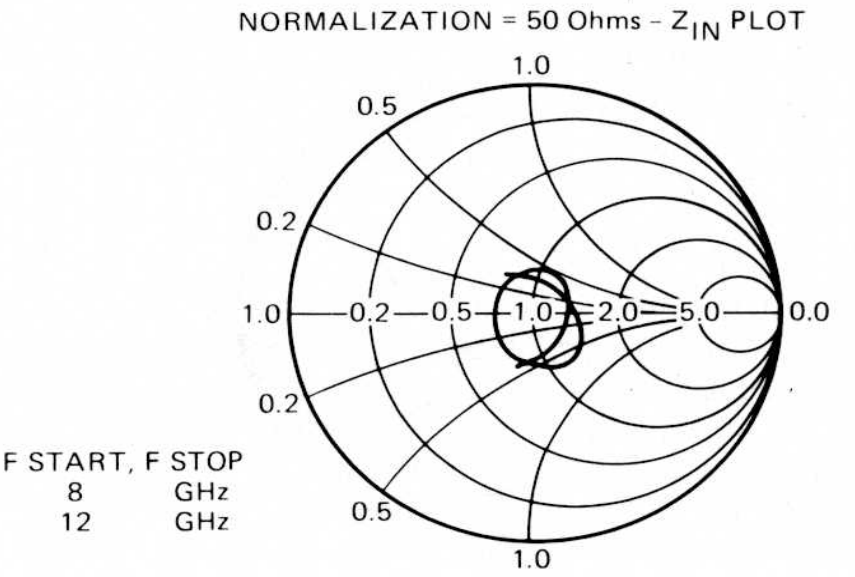

c) INPUT MATCH PERFORMANCE

Figure 8.29 Input matching network.

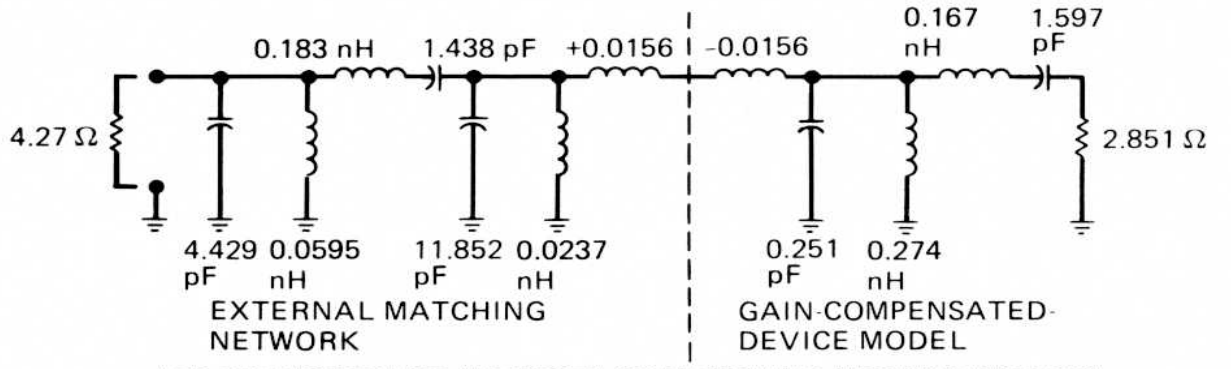

a) BP TRANSFORMED INTERSTAGE MATCHING NETWORK/MODEL

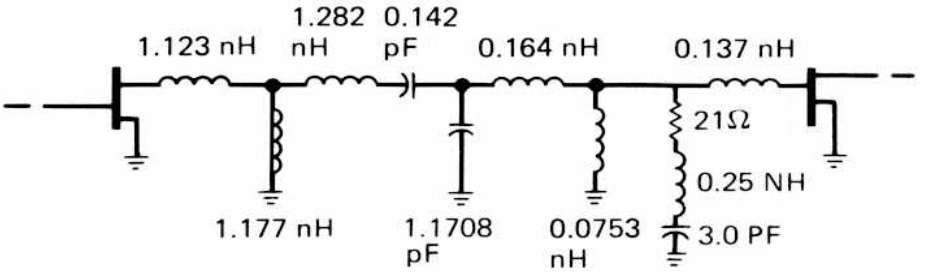

b) COMPLETED INTERSTAGE NETWORK, AFTER NORTON TRANSFORMER INSERTION

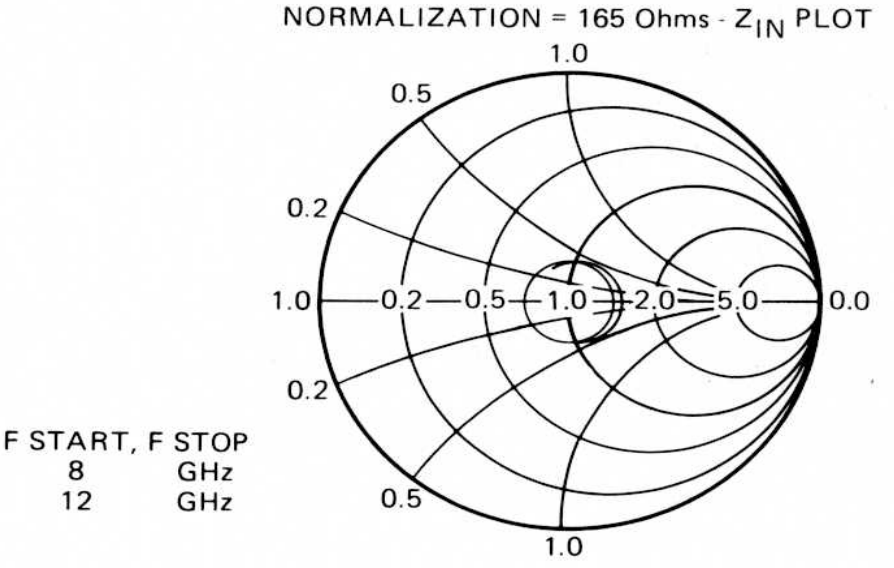

IMPEDANCE CHART

c) INTERSTAGE MATCH PERFORMANCE

Figure 8.30 Interstage matching network.

The bandpass transformed interstage matching network is illustrated in Fig. 8.30a. Two inductive Norton transformers are then inserted to obtain the 165 Ω and 0.114 pF source (FET drain) model (Fig. 8.30b). Interstage match performance is shown in Fig. 8.30c. This represents the power match provided to the driver stage, since a large-signal output model was used.

Output Match

$$N = 4$$

$$Q_{\text{Source}} = 1.164$$

$$a = 0.928$$

$$b = 0.521$$

$$\text{VSWR}_{\text{Bode}} = 1.00{:}1$$

$$\text{VSWR}_{\text{max}} = 1.11{:}1$$

$$\text{VSWR}_{\text{min}} = 1.03{:}1$$

$$g_0 = 1.0$$

$$g_1 = 0.475$$

$$g_2 = 0.388$$

$$g_3 = 1.107$$

The bandpass transformed output matching network is illustrated in Fig. 8.31a. Since the topology here is dictated by the necessity of a parallel device model, the only available Norton transformation is downward (with this $N = 4$ case). Upward transformation is desired; so, the order could be increased to $N = 6$. Since the external load is 50 Ω to within a VSWR of 1.03:1, no Norton will be used. The power match provided by this circuit is can be seen in Fig. 8.31b.

The overall two-stage amplifier circuit and response are shown in Fig. 8.32. We have systematically and optimally obtained this design. It is important to note that no numerical optimization was used with this procedure. Monolithic realization of this lumped design is straightforward with quasi-lumped or distributed elements. The conversion of lumped designs into MMIC-compatible form is discussed in the next section.

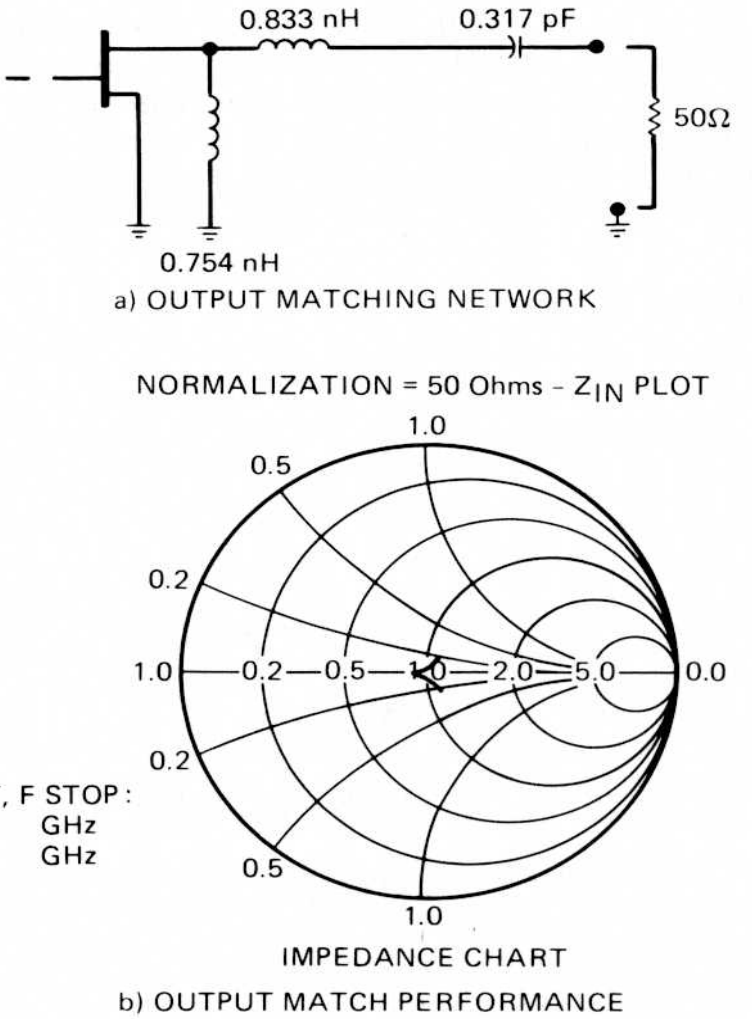

Figure 8.31 Output matching network.

8.5 MMIC CIRCUIT ELEMENTS

This section addresses the realization of passive circuit elements in a monolithically integrated form. We will begin this discussion with a bold statement: "*Ideal lumped elements do not exist*!" Distributed effects are always present. "Lumped" inductors and capacitors will always self-resonate at some frequency. Similarly, reactive effects can always be found in resistors. A key to achieving good equivalent lumped-element performance is small element size compared with the operating wavelength.

8.5.1 Transmission-line Element Approximations

A short segment of transmission line can be used to approximate an inductor or capacitor, depending on its characteristic impedance and how it is used (interconnection topology). For purposes here, we will consider lossless quasi-TEM line representations. Lossy lines can easily be substi-

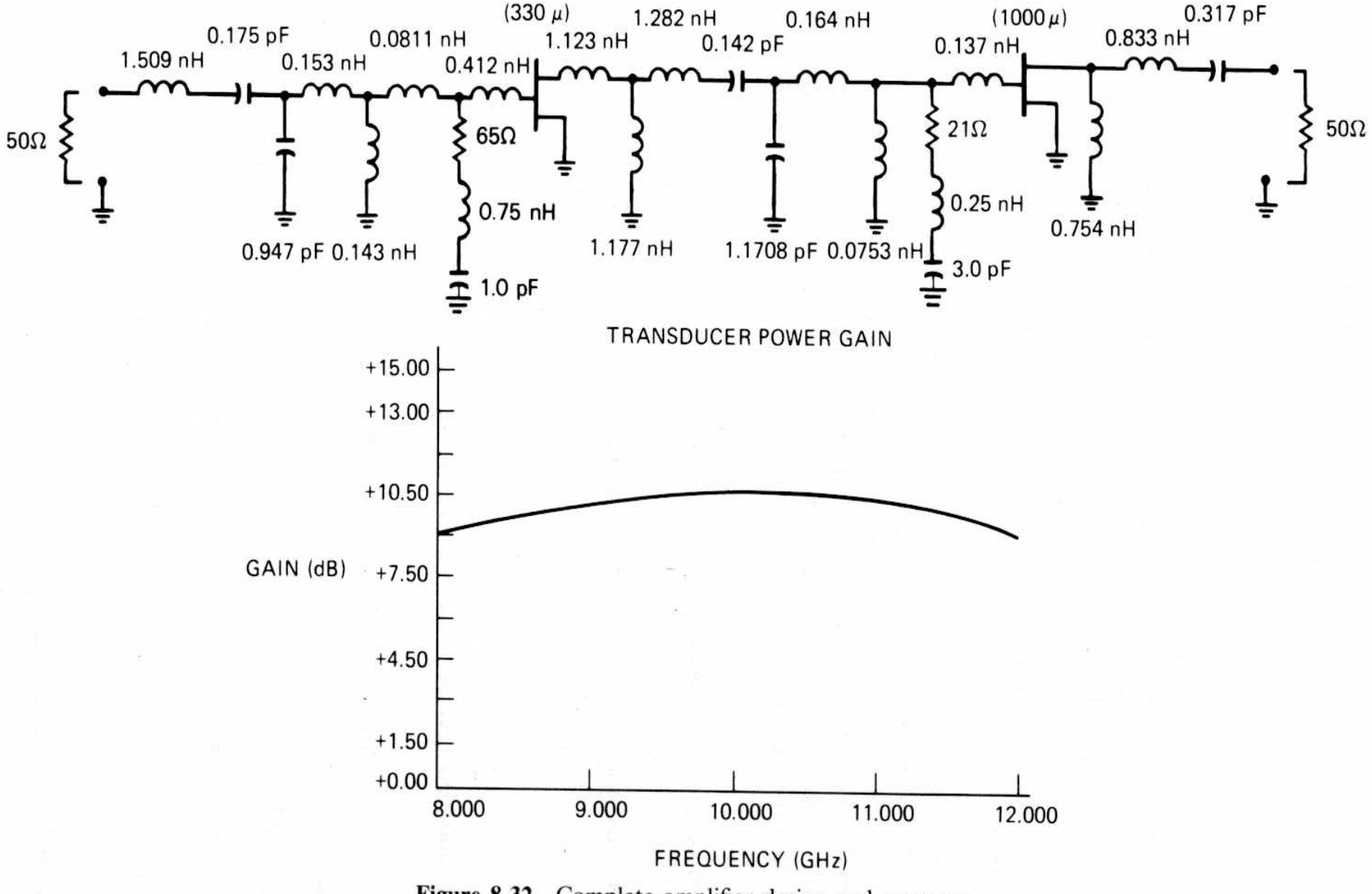

Figure 8.32 Complete amplifier design and response.

tuted. The quasi-TEM assumption is good, since microstrip lines are by far the preferred media for MMICs. On an incremental basis, the characteristic impedance Z_0 of the line is given by

$$Z_0 = \sqrt{\frac{L}{C}} \tag{61}$$

In Eq. (61), L and C are the incremental series inductance and shunt capacitance per unit length, respectively. The higher the characteristic impedance, the more series inductance and less shunt capacitance per unit length are seen. Lumped inductor behavior can be approximated if a sufficiently large Z_0 is used. Alternatively, from low Z_0 lines, lumped approximations for capacitors can be obtained. The conversion relationships are obtained by coefficient matching Y- or Z-parameter representations of transmission-line segments with those of third-order lowpass LC models. The equivalent forms are depicted in Fig. 8.33. Clearly, a series inductor is represented by the pi-section of Fig. 8.33a. In a similar manner, a short-circuited shunt stub can be used to approximate a shunt inductor. The T section of Fig. 8.3b allows a practical shunt capacitor approximation. Series capacitors are a bit more difficult where microstrip lines are used. However, the "lumped"-overlay-type capacitor can be modeled quite well with this

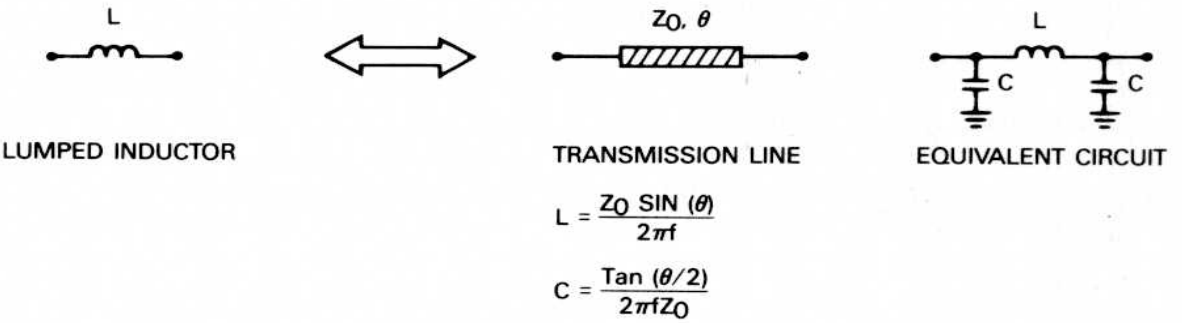

a). TRANSMISSION LINE INDUCTOR APPROXIMATION

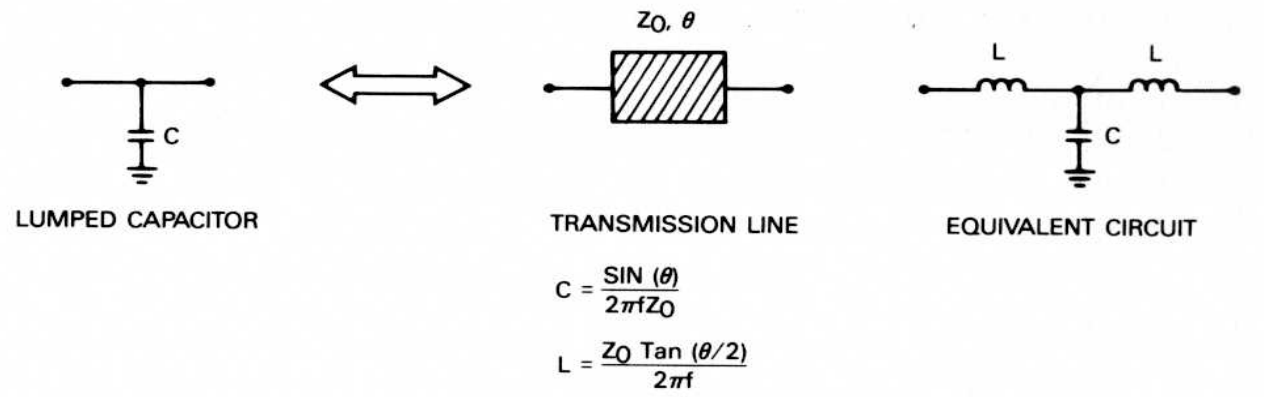

b). TRANSMISSION LINE CAPACITOR APPROXIMATION

Figure 8.33 Transmission-line equivalents for lumped elements.

method, as will be discussed in the next section. Microstrip lines offer characteristic impedances between 15 and 100 Ω on 75–100 μm GaAs substrates. Good lumped equivalent performance can be obtained when transmission-line length is less than 30°.

8.5.2 Lumped Capacitors

Monolithic circuit realization of lumped capacitors is commonly fabricated with several geometries. The most often used form is called the "overlay." To a much lesser extent, the so-called "interdigitated" geometry is employed. Most contemporary designs use the overlay exclusively, since it offers a lower shunt parasitic capacitance, a much wider range of practical realizations, and more compact size. Therefore, our discussion will be directed to this geometry. For more information about interdigital capacitors, see Alley [18] and Esfandiari [19]. When either of the capacitor forms is used as a series of dc blocking elements, a parasitic shunt capacitance is also seen. This is due to the electric field path through the GaAs substrate. Of course, if one side of the capacitor is to be grounded, then this additional capacitance can easily be included into the capacitor design.

Overlay capacitors are fabricated by depositing a thin-film dielectric layer between thin-film metal plates. This is illustrated in Fig. 8.34. Typical dielectric layer thicknesses are between 0.2 and 0.25 μm. Common dielectric materials are silicon nitride (Si_3N_4), silicon dioxide (SiO_2), and tantalum pentoxide (Ta_2O_5). When SiO_2 or $Ta2O_5$ is used, the result is sometimes called a metal–oxide–metal (MOM) capacitor. Dielectric constant properties are as follows:

Material	Dielectric Constant	Temperature Coefficient
Si_3N_4	6–7	25–35
SiO_2	4–5	100–500
Ta_2O_5	20–25	0–200

High-quality MMIC capacitors must exhibit low microwave energy loss, high breakdown field capability, capacitance stability with temperature, and good film integrity (low pinhole density and stability). Clearly, the dielectric film plays a central role in determining the performance in each of these categories.

Conductor losses are also important in determining the microwave Q-factor. This can be seen in the overlay capacitor models of Fig. 8.35.

Two modes must be allowed, since the overlay structure is suspended over a second dielectric layer (the GaAs substrate). The odd-mode characteristic impedance is equivalent to that of a microstrip line of the same width and half the dielectric thickness as the capacitor. The even-mode characteristic impedance is set by the capacitance of the microstrip mode through the GaAs substrate. When the coupled line model of Fig. 8.35a is converted

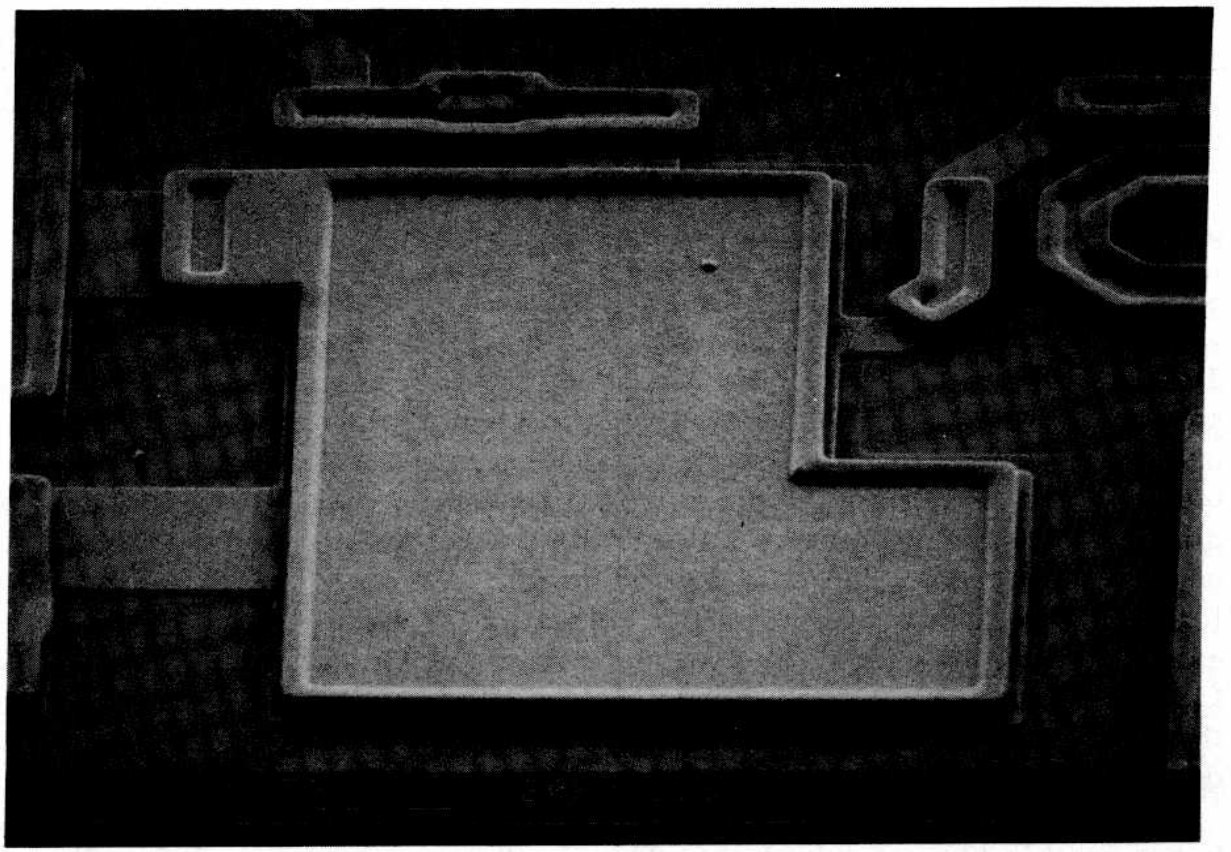

Figure 8.34 Scanning electron micrograph (SEM) of MMIC overlay capacitor.

Fig. 8.35a is converted into a lumped approximation, the model forms of Fig. 8.35b and c are obtained. The transmission-line representation method which was discussed in Section 8.5.1 is applicable here if lossy lines are used. The applicable equations are

$$C_1 = C_3 - \text{Parallel plate substrate capacitance}$$

$$C_2 = \frac{\sin(\Theta)/(\omega Z_{0o}) - \sin(\Theta)/(\omega Z_{0e})}{2}$$

$$C_3 = \frac{\sin(\Theta)}{\omega Z_{0e}}$$

$$L_S = \frac{Z_{0o}\tan(\Theta/2)}{\omega}$$

$$R_S = \frac{Z_{0o}\tan(\Theta/2)}{Q_{\text{even}}}$$

$$R_P = \frac{2Z_{0o}Q_{\text{odd}}}{\sin(\Theta)}$$

It is interesting to note that accurate modeling of "lumped" capacitors has necessitated a distributed model.

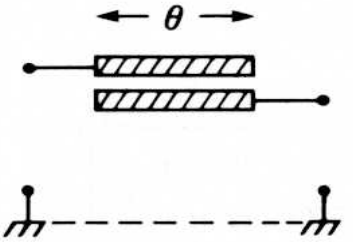

a). ASSYMETRIC BROADSIDE COUPLED LINE MODEL

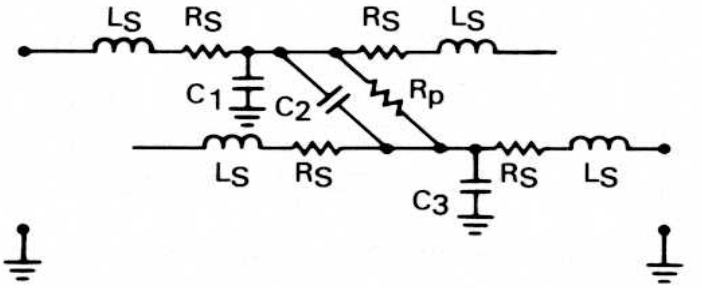

b). LUMPED EQUIVALENT OF BROADSIDE COUPLED LINE MODEL

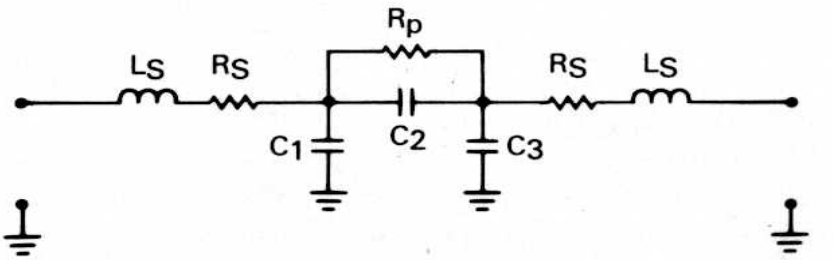

c). SIMPLIFIED LUMPED EQUIVALENT MODEL

Figure 8.35 Circuit models for MMIC overlay capacitors.

8.5.3 Lumped Inductors

When relatively large inductance values are required, uncoupled transmission lines of the form described in Section 8.5.1 are not always useful. This limitation is set by the maximum practical realizable microstrip characteristic impedance. The rectangular spiral configuration shown in Fig. 8.36a offers a means of exceeding the uncoupled-line inductance limit. Additionally, more efficient utilization of MMIC surface area results, when compared with meander-line or S-line ("uncoupled") configurations. The notation for the present discussion is also indicated in Fig. 8.36a. The horizontal lines are labeled H_x and the vertical lines labeled V_x.

Two modeling approaches for rectangular spiral inductors will now be discussed. The modified Grover [20] method used by Greenhouse [21] is

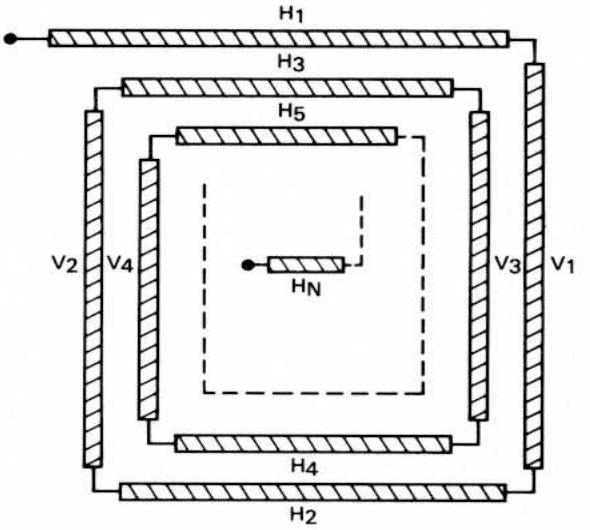

a). RECTANGULAR "SPIRAL" CONFIGURATION/NOTATION

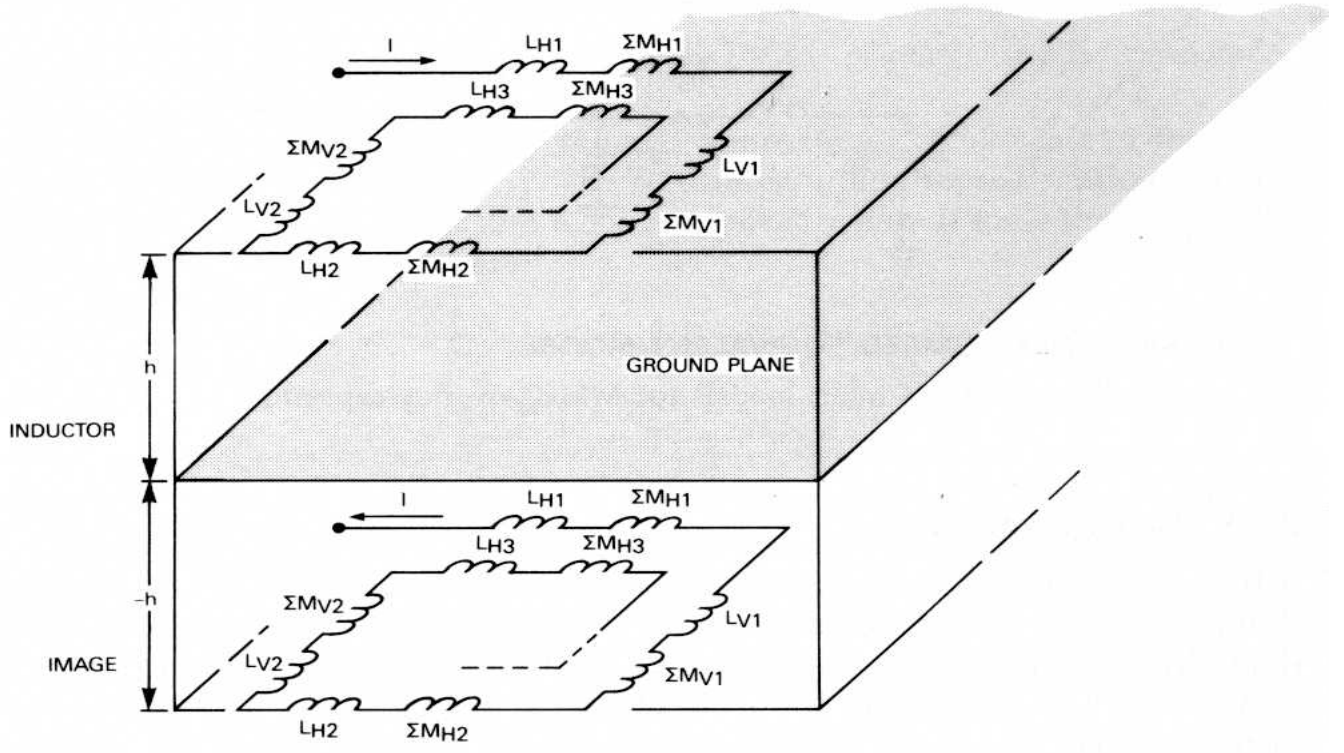

b). GREENHOUSE/GROVER MODEL

Figure 8.36 Rectangular spiral inductor circuit models.

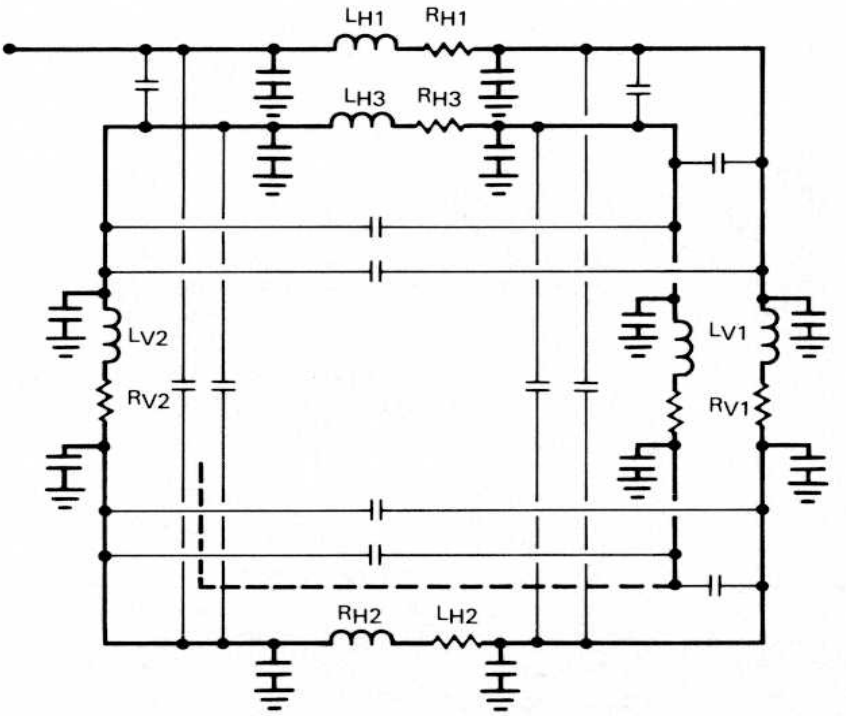

c). LUMPED EQUIVALENT REPRESENTATION OF TRANSMISSION LINE MODEL FOR RECTANGULAR "SPIRAL"

Figure 8.36 continued

illustrated in Fig. 8.36b. Only magnetic interactions are considered in this model. Ground-plane effects are equivalently represented by an antiphased image, separated by a distance of twice the ground-plane spacing. The total inductance is equal to the sum of the segment self-inductances added to the sum of the mutual inductive contributions. These effects are shown separately in Fig. 8.36b for each inductor segment. For MMIC applications, the self-inductances are approximately given by

$$L\ (\mu\text{H}) = 0.002a\left[\ln\left(\frac{2a}{b}\right) + 0.5005 + \frac{b}{3a}\right] \tag{62}$$

where a = length and b = width of the line segment in centimeters. The mutual inductance between two segments is approximated by

$$M\ (\mu\text{H}) = 2a\left[\ln\left(\frac{a}{d} + 1 + \frac{a^2}{d^2}\right) + \left(1 - 1 + \frac{a^2}{d^2}\right)\frac{d}{a}\right] \tag{63}$$

where d = distance between centers. The mutual inductive contribution to each segment is due to the summation over all parallel-line segments. This includes all image-line segment contributions. More details about this method can be found in Greenhouse [21]. Good results can be obtained for moderate-to-small rectangular spirals, since the current in each line segment

Figure 8.37 SEM of an MMIC spiral inductor.

is approximately the same and near-resonance effects (due to distributed capacitance) are minimal.

For large rectangular spiral inductors, where phase shift between line segments become significant, coupled transmission lines provide a more accurate model. Similar to the application of transmission-line (T) equivalent circuits from Section 8.5.1 to overlay capacitors in Section 8.5.2, pi equivalent circuits can be used to model the coupled-line segments. This approach can be seen in Fig. 8.36c. The adjacent even-mode impedance and line-segment lengths are used to determine the series inductance and even-mode shunt capacitance for each segment. This can be done with the equations of Fig. 8.33a. Losses can be represented by the series resistance in each segment. The coupling capacitances are then determined by calculating half the difference between the odd-mode and even-mode shunt capacitance.

A scanning electron micrograph of an MMIC rectangular spiral inductor is shown in Fig. 8.37.

8.5.4 Lumped Resistors

The thin-film monolithic resistor is realized either by isolating a substrate region that carries a conductive epitaxial layer or by vacuum deposition of a

metallic conductive film on the substrate. The isolation process in the semiconductor resistors is achieved by either implantation or mesa etch. Metal films are usually preferred, however, since semiconducting films exhibit nonlinear behavior at high current levels. Also, semiconductor resistors in which a relatively low value of resistance is desired also require that particular attention be given to resistance contributed by the ohmic contact.

The most commonly used thin-film resistor materials are tantalum nitride and nichrome. Resistivities for these materials are 280–300 and 60–600 $\Omega \cdot$ cm, respectively. The first-order calculation for a films resistance is expressed in

$$R = \rho \frac{\text{length}}{\text{area}} \tag{64}$$

where ρ is the bulk resistivity (in $\Omega \cdot$ cm). When the thickness of the film is identified, the resistivity is sometimes specified as a sheet resistivity ρ_S (in $\Omega/\square$). In this manner, Eq. (65) is obtained. Clearly, this form is of great practical use, since one must only count the number of squares (length to width ratio) that comprise the resistive path to determine the resistance.

$$R = \rho \frac{\text{length}}{\text{area}} = \frac{\rho_S \text{ length}}{\text{width}} \tag{65}$$

$$\rho_S = \frac{\rho}{\text{thickness}} \tag{66}$$

When corners or steps are encountered, the number of squares in the path must be modified to allow for the discontinuity. For example, a uniform right-angle bend has effectively 0.559 squares of path length. A nonuniform right-angle bend of aspect ratio a has an effective path length given by Eq. (67). Keep in mind that these are dc current crowding effects. We have yet to apply the rf effects.

$$\text{Length} = \frac{1}{a} - \frac{2\ln[4a/(a^2+1)]}{\pi} + \frac{(a^2-1)\cos^{-1}[(a^2-1)/(a^2+1)]}{a\pi} \tag{67}$$

It should come as no surprise to find that "lumped" thin-film resistors are no more ideal than were the capacitors and inductors of the previous two sections. Since thin-film resistors occupy surface area over the GaAs substrate, distributed capacitance to the ground plane is present. Similarly, the path length in the direction of current flow contributes a series inductance, along with the desired resistance. If the resistor film is laser-trimmed, the modified current flow path must be considered in order to determine its microwave behavior. The inductive and capacitive branches are in the necessary lowpass form for application of the equations from Fig. 8.33 (Section 8.5.1). This approach to modeling thin-film resistors will now be discussed.

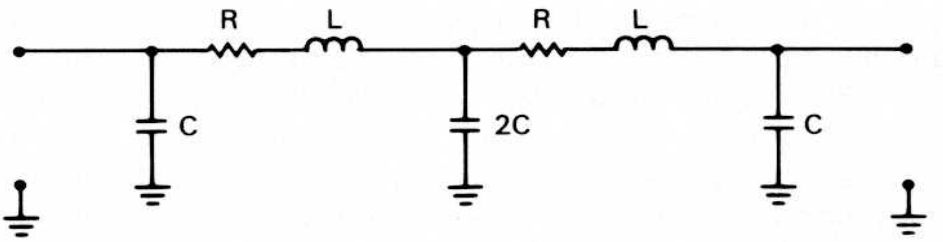

Figure 8.38 Equivalent circuit for thin-film resistors.

When a thin-film resistor is viewed as a lossy transmission line that has conceptually been partitioned into two cascaded sections, the lumped equivalent form illustrated in Fig. 8.38 is obtained. The inductance value L is calculated from the pi model in Fig. 8.33 for half the resistors electrical length. Similarly, C is determined from the same set of equations. The total thin-film resistance is divided by two to obtain R in Fig. 8.38. This two section (fifth-order) approach is valid as long as the resistor path is less than 90° in effective length. For longer structures, the number of sections in the model can be increased; so, 45° per section is not exceeded.

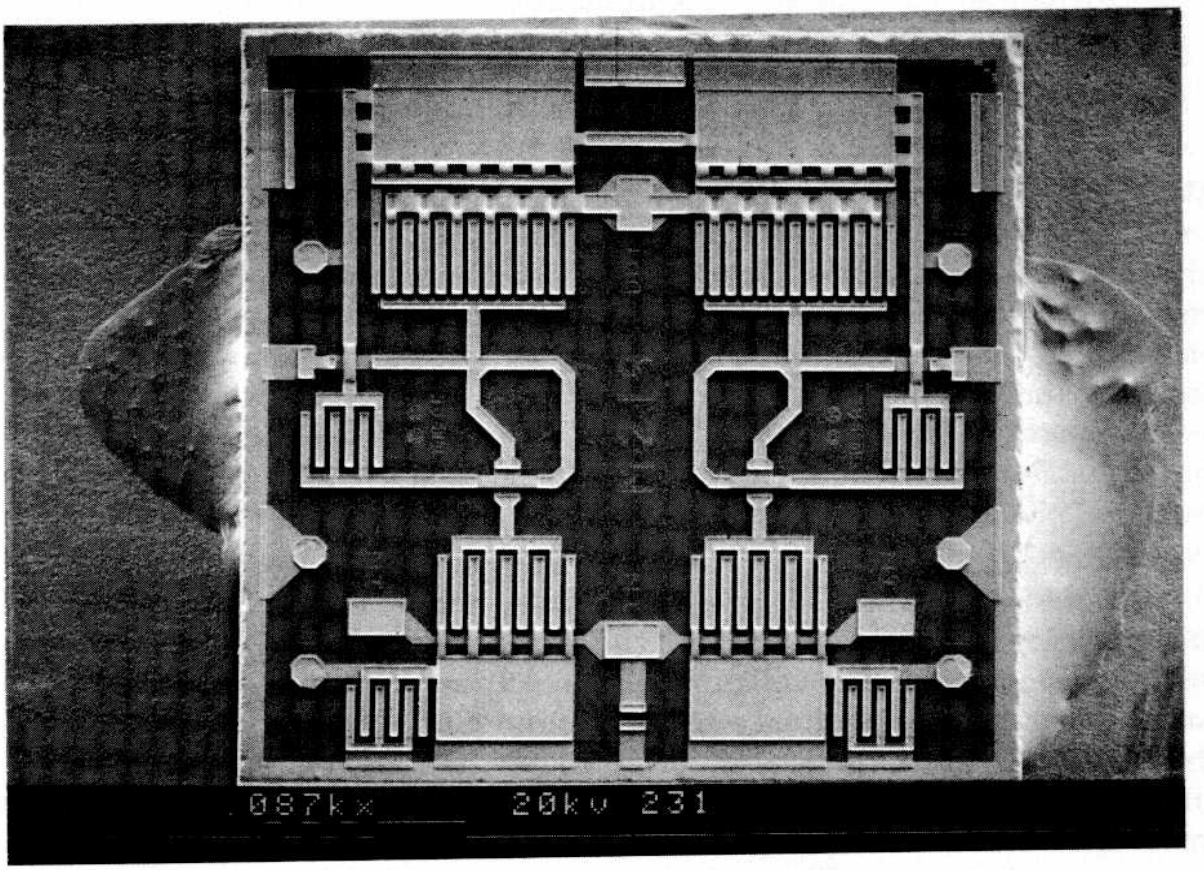

a) TWO FET STAGES WITH INTERSTAGE MATCHING AND SELF-BIAS RESISTORS.
—ILLUSTRATES: TRANSMISSION LINE INDUCTORS,
OVERLAY CAPACITORS, AND
THIN-FILM RESISTORS.

Figure 8.39 Application of lumped elements to MMICs.

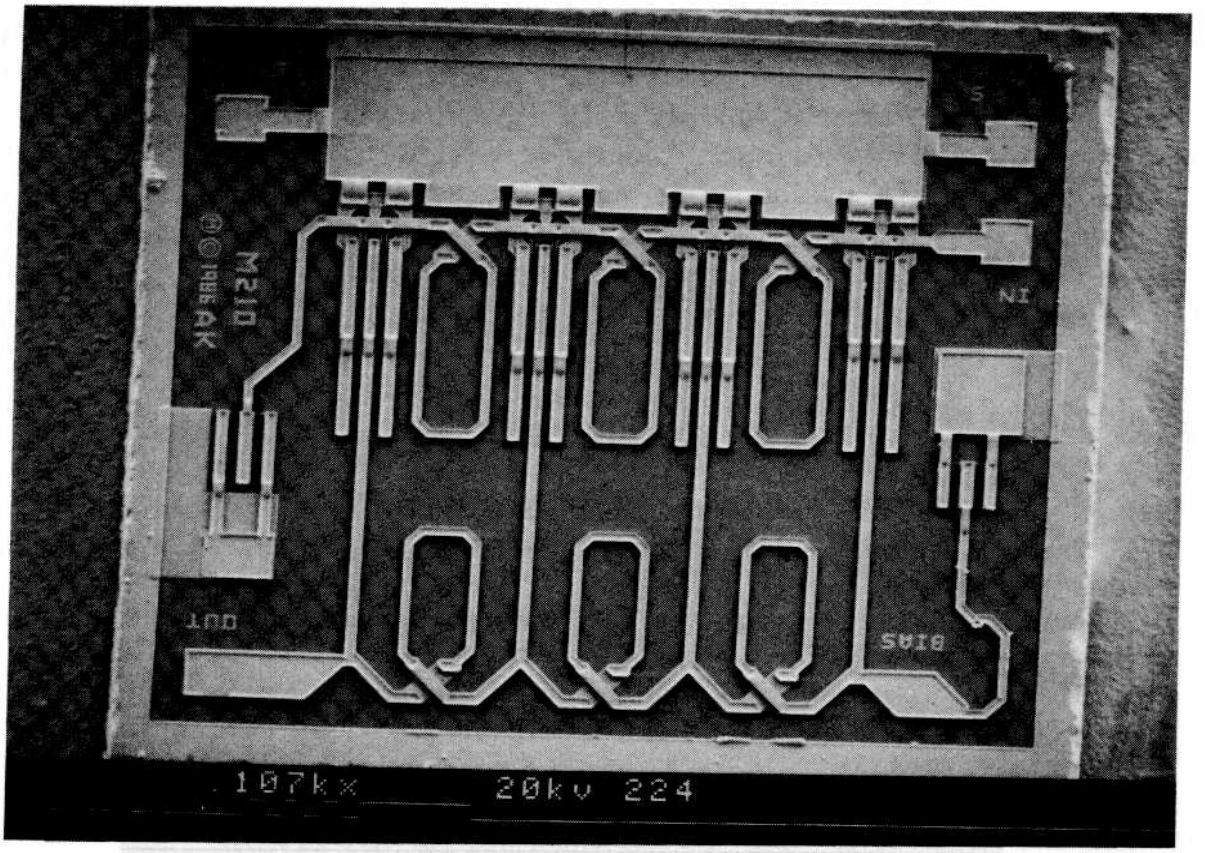

b) FOUR FET STAGES OF DISTRIBUTED AMPLIFICATION
—ILLUSTRATES: SPIRAL INDUCTORS,
OVERLAY CAPACITORS,
AND THIN-FILM RESISTORS.

Figure 8.39 continued

8.6 SUMMARY

This chapter began with a discussion of similarities in various FET amplifier applications from the standpoint of matching network design constraints. It was shown that the needs of each application could be reduced to the same problem: obtaining a network that provides a desired driving-point impedance behavior.

Much of the material in the chapter was accordingly devoted to presenting a systematic method for obtaining optimum matching networks. An understanding of the limits of achievable match bandwidth performance is essential before a design begins, so a detailed discussion of Bode's limit analysis was included. The methods presented did not require numerical optimization nor other computer support to obtain solutions; thus, sufficient detail was included for application by the reader. To facilitate an understanding of these techniques and their application to practical design problems, a two-stage power amplifier design example was included.

The material that followed the design example was directed to the realization of FET microwave amplifier designs in a monolithic form. The

use of transmission lines to approximate inductors and capacitors was first presented. Next, "lumped" inductors, capacitors, and resistors were examined. In each case, it was seen that nonideal distributed effects were needed to model the element adequately. There are no truly lumped elements! The most useful forms were discussed. These included overlay capacitors, rectangular spiral inductors, and metallic thin-film resistors. Figure 8.39 illustrates application of these elements in MMIC realizations. (Photos courtesy of AVANTEK, Inc.)

REFERENCES

1. R. S. Carson, "High Frequency Amplifiers." Wiley, New York, 1975.
2. "S-Parameter Design," HP Appl. Note 154. April 1972. (Hewlett Packard in house publication)
3. H. W. Bode, "Network Analysis and Feedback Amplifier Design." Van Nostrand, New York, 1945.
4. R. M. Fano, "Theoretical Limitations on the Broadband Matching of Arbitrary Impedances," MIT Tech. Rep. No. 41. Massachusetts Institute of Technology, Cambridge, 1948.
5. G. L. Matthaei, Synthesis of Tchebycheff impedance-matching networks, filters, and interstages. *IRE Trans. Circuit Theory* **3**, 163–172 (1956).
6. L. Weinberg, "Network Analysis and Synthesis." McGraw-Hill, New York, 1962.
7. R. Levy, Explicit formulas for Chebyshev impedance matching networks, filters, and interstages. *Proc. Inst. Electr. Eng.* **111**, 1099–1106 (1964).
8. E. Green, "Amplitude-Frequency Characteristics of Ladder Networks." Marconi's Wireless Telegraph Co., Essex, England, 1954.
9. H. Takahasi, On the ladder-type filter network with Tchebyshev response. *J. Inst. Electr. Commun. Eng. Jpn.* **34** No. 2 (1951).
10. A. I. Zverev, "Handbook of Filter Synthesis." Wiley, New York, 1967.
11. T. R. Apel, "Bandpass Matching Networks Can Be Simplified By Maximizing Available Transformation," pp. 105–117. Microwave Systems News, Palo Alto, CA, 1983.
12. E. Christian and E. Eisenmann, Broad-band matching by lowpass transformations. *Allerton Conf. Circuit Syst. Theory 4th, 1966* pp. 155–164 (1966).
13. G. L. Matthaei, Tables of Chebyshev impedance-transforming networks of low-pass filter form. Proc. *IEEE* **52**, 939–963 (1964).
14. R. M. Cottee and W. I. Joines, Synthesis of lumped and distributed networks for impedance matching of complex loads *IEEE Trans. Circuits Syst.* **CAS-26**, 316–329 (1979).
15. E. G. Cristal, Tables of maximally flat impedance transforming networks of low-pass filter form. *IEEE Trans. Microwave Theory Tech.* **MTT-13**, 693–695 (1965).
16. P. J. T. Mellor, Improved computer-aided synthesis tools for the design of matching networks for wide-band microwave amplifiers. *IEEE Trans. Microwave Theory Tech.* **MTT-34**, 1276–1281 (1986).
17. T. R. Apel, "One-Port Impedance Models Prove Useful for Broadband RF

Power Amplifier Design," pp. 96–105. Microwave Systems News, Palo Alto, CA, 1984.
18. G. D. Alley, Interdigital capacitors and their application to lumped element microwave integrated circuits. *IEEE Trans. Microwave Theory Tech.* **MTT-18**, 1028–1032 (1970).
19. R. Esfandiari, P. W. Maki, and M. Siracusa, Design of interdigitated capacitors and their application to gallium arsenide monolithic filters. *IEEE Trans. Microwave Theory Tech.* **MTT-31**, 57–64 (1983).
20. F. W. Grover, "Inductance Calculations: Working Formulas and Tables." Van Nostrand, New York, 1946.
21. H. M. Greenhouse, Design of planar rectangular microelectronic inductors. *IEEE Trans. Parts, Hybrids, Packag.* **10**, 101–109 (1974).